Classification of Alpine South Foehn based on five years of km-scale analysis data

Lukas Jansing[1], Lukas Papritz[1], Bruno Dürr[2], Daniel Gerstgrasser[3], and Michael Sprenger[1]

[1]Institute for Atmospheric and Climate Science, ETH Zürich, Zurich, Switzerland
[2]Sunergy GmbH, Degersheim, Switzerland
[3]MeteoSwiss, Zurich, Switzerland

Correspondence: Lukas Jansing (lukas.jansing@env.ethz.ch)

Abstract. It has long been recognized that a rich variety of Alpine South Foehn flavors exists that is related to varying flow conditions above crest level, the presence and intensity of orographic precipitation on the Alpine south side, and the Po Valley stratification. This study presents a systematic five-year climatology of different Foehn types. The classification relies on 2'329 Foehn hours, which are diagnosed using a station-based Foehn index for Altdorf in the Swiss Reuss Valley. Operational

5   analyses at 1-km horizontal resolution are employed to classify Foehn hours with a decision tree that is based on Foehn forecasting experience. Mean wind direction and speed in a circle with 100 km radius centered around Altdorf are considered to differentiate between three main Foehn types (*Deep Foehn*, *Shallow Foehn*, *Gegenstrom Foehn*). In addition, upstream precipitation and its extent beyond the Alpine crest are used to distinguish three *Deep Foehn* subtypes (*Dry Foehn*, *Moist Foehn*, *Dimmer Foehn*).

10   The main Foehn types differ distinctively in the synoptic conditions over the Alps. During *Deep Foehn*, pronounced south-westerlies ahead of an upper-level trough induce upstream orographic precipitation. *Shallow Foehn*, in turn, is associated with cross-Alpine temperature differences that provoke a gap flow. The *Gegenstrom Foehn* type is also restricted to major gaps, but a strong westerly flow prevails above crest level. The *Deep Foehn* subtypes primarily differ in terms of the upper-level trough. While a weaker trough and the influence of an upper-level ridge over the Mediterranean inhibit precipitation (*Dry Foehn*),

15   a deeper trough which is closer to the Alps induces stronger crest-level winds and intense precipitation on the Alpine south side (*Dimmer Foehn*). The different Foehn types are found to strongly affect the local characteristics at Altdorf, which are investigated using station measurements.

Backward trajectories from Altdorf are calculated for each of the Foehn hours and used to define three clusters of air parcels depending upon their upstream thermodynamic evolution. Trajectories in cluster 1 are diabatically heated and transported

20   within a low-level easterly barrier jet in the Po Valley prior to their ascent to crest level. They constitute the main precipitating airstream and, hence, are of key importance for *Moist Foehn* and *Dimmer Foehn*. Cluster 2 and 3 trajectories are subject to weak diabatic heating or even diabatic cooling. They originate from southerly to southwesterly regions and from either slightly below or above crest level. Accordingly, these air parcels are associated with little to no precipitation and as such, they take a key role for *Dry Foehn*, *Shallow Foehn* and *Gegenstrom Foehn*. Furthermore, these three Foehn types feature a pronounced

25   stable layer over the Po Valley, which, to some extent, inhibits air parcels to ascend from lower levels.

In summary, the study introduces a systematic classification of South Foehn using state-of-the-art data sets. It concludes by setting the new classification into a historic context and revisiting the rich body of literature with respect to different Alpine South Foehn types. In particular, analogies and discrepancies to the existing conceptual models of 'Swiss Foehn' and 'Austrian Foehn' are discussed.

1 Introduction

Foehn, originating from the latin *favonius* (e.g., Sprenger et al., 2016), represents a generic term for downslope winds and windstorms in the lee of mountains. These strong and often gusty winds are associated with a distinct warming and a decrease in relative humidity of the air on the lee-side of the orographic barrier (e.g., Richner and Hächler, 2013). The Alpine Foehn profoundly impacts societies in the affected regions. For example, Foehn occurrence enhances the risk for forest fires (Zumbrunnen et al., 2009; Wastl et al., 2013). At the same time, the Foehn-induced microclimate can benefit agricultural production, e.g., viticulture in Foehn valleys (Walker and Ruffner, 1998). Accordingly, this archteypal wind phenomenon has already piqued the curiosity of the 19th century Swiss naturalists. For example, Escher von der Linth attributed the occurrence of ice ages to the lack of Foehn winds during these periods (the Sahara theory; see, e.g., Lehmann, 1937). Additional, sometimes fierce, disputes among scientists concerned the reason for the exceptional warmth of the Foehn air, as well as the driving mechanism for the descent into the Foehn valleys (see, e.g., Steinacker, 2006, for a summary of different Foehn theories).

Alpine South Foehn events are associated with characteristic synoptic situations. The generic situation is that an upstream upper-level trough induces southwesterly to southerly large-scale flow towards the Alps. Meanwhile, at the surface, an extra-tropical cyclone and its attendant frontal system approach Central Europe. As a result, a pressure gradient builds up across the Alps and Foehn winds break through on the Alpine north side. Detailed descriptions of the synoptic evolution of so-called *Deep Foehn* events can be found in the literature (e.g., Burri et al., 1999; Richner et al., 2006; Hächler et al., 2011; Jansing and Sprenger, 2022). With respect to *Deep Foehn*, Burri et al. (1999) differentiates between 'pre-frontal Foehn', where short-lived Foehn episodes are terminated by rapidly propagating cold fronts (e.g., Hächler et al., 2011), and long-lasting Foehn situations related to stationary upper-level troughs ('trough Foehn' situations), where the upstream trough over Western Europe can remain quasi-stationary for up to several days (e.g., Jansing and Sprenger, 2022).

However, even early on, scientists also recognized the existence of different Foehn varieties and different stages within a Foehn event. In fact, Hann (1885) already emphasized that Foehn can occur without upstream precipitation (in our terminology, we refer to it as *Dry Foehn*), and oftentimes Foehn breakthrough precedes the formation of orographic precipitation. Ficker (1910) divides the typical Foehn event into two stages: During the 'anticyclonic stage', while Foehn winds are already established on the Alpine north side, air does not ascend on the south side. Instead, the free troposphere is separated from the air below by an inversion layer, above which southerly winds and very low humidity values are observed. While a Foehn event can terminate at this stage, it is usually followed by the 'stationary stage', where upstream precipitation starts to form and the characteristic 'Foehn wall' (i.e., the prominent wall formed by upstream clouds over the crest as viewed from the lee) establishes. According to Kuhn (1984), Billwiller first introduced the term 'anticyclonic Foehn', but interpreted it as the subsidence

of air within an anticyclone situated over the Alpine ridge. For this reason, Gubser (2006) does not classify this Foehn type or

60   stage as a Foehn wind. On the other hand, in most publications, 'anticyclonic Foehn' or the 'anticyclonic stage' is interpreted as the Foehn phase without upwind precipitation and little to no cloud formation (e.g., Burri et al., 1999; Gerstgrasser, 2017), often followed by the 'stationary stage' or 'cyclonic stage' (see also in Frey, 2007). An example following this evolution is the 'once-in-a-century Foehn event' ('Jahrhundertföhn') from 7th and 8th November 1982 as described by Frey (1984), where a record-breaking cross-Alpine pressure difference of 24 hPa was observed.

65   Another Foehn variety, primarily discussed by Swiss Foehn researchers, concerns the so-called 'dimmerfoehn', in the following referred to as *Dimmer Foehn* (Richner and Dürr, 2015). Streiff-Becker (1933) describes the local meteorological conditions associated with *Dimmer Foehn*: The Foehn wall extends unusually far beyond the main Alpine crest. As a consequence, the otherwise dry Foehn regions appear hazy due to the presence of humid and cloudy air. Oftentimes, precipitation falls into the Foehn valley atmosphere and induces evaporative cooling, which strongly reduces the dewpoint depression (Richner and

70   Hächler, 2013). Yet another peculiarity with respect to *Dimmer Foehn* is related to the shift in its northward extent: As the upper part of the Foehn valleys is situated within the humid air being advected over the main crest, the Foehn reaches the ground further down-valley compared to the normal *Deep Foehn* (Streiff-Becker, 1947). According to Streiff-Becker (1947), the Foehn also advances unusually far north. While *Dimmer Foehn* is regarded as a rare Foehn variety with a local lee-side impact, the synoptic conditions nonetheless deviate from *Deep Foehn*. The upstrem low pressure system tends to be closer to

75   the Alps and, as a result, large-scale southwesterlies or southerlies above crest level are stronger. Streiff-Becker (1947) also emphasizes the frequent presence of secondary lee-cyclones during such events. So far, however, *Dimmer Foehn* has solely been investigated in single case studies (e.g., Zängl and Hornsteiner, 2007), and no systematic evaluation of the characteristic synoptic to mesoscale conditions during *Dimmer Foehn* has been performed.

    The aforementioned Foehn types share a common characteristic, namely the presence of an upstream disturbance inducing

80   flow with a southerly component towards the Alps. Besides, however, it has also been noticed, primarily by Austrian Foehn researchers, that South Foehn can likewise establish without the presence of a pronounced cross-Alpine flow component above crest level. In his textbook, Hann (1901) briefly mentions the occurrence of Foehn due to smaller cross-Alpine pressure differences, when no southwesterly winds are present in the Alpine foreland. Ficker (1931) describes the development of Foehn winds, while above crest-level winds are weak and, sometimes, even from a northerly direction. To our knowledge, the first

85   appearance of the term *Shallow Foehn* occurs in Kanitscheider (1932), as he depicts several Foehn cases with a limited vertical extent of the southerly winds in the Innsbruck region, whereas weaker westerlies prevail above a certain level. Seibert (1990) defines *Shallow Foehn* as "... a foehn with all typical properties in the valleys, but without pronounced southerly wind component at upper levels (above crest height).". Applying a range of criteria, roughly 10% of all Foehn hours in Innsbruck are classified as *Shallow Foehn*. However, it is unclear how frequently this Foehn type occurs in the Swiss Alps. Additionally, a

90   mechanistic explanation is included in Seibert (1990): *Shallow Foehn* is regarded as a result of cross-Alpine temperature and pressure differences of the contrasting low-level air masses on the Alpine north and south side, respectively. These, in turn, induce a hydraulic 'compensation flow' through major gaps along the Alpine transect. In fact, Mayr and Armi (2008) extend this line of reasoning even further, by arguing that the presence of north-south temperature differences are a necessary condition for

the formation of *Shallow Foehn* as well as *Deep Foehn*, while a southerly flow component merely imposes a modification to the

95 conditions responsible for Foehn formation. They link the build-up of cross-Alpine temperature gradients to the advection of cold and warm air around the eastern and western edge of the Alps, respectively. The initial driver of the temperature advection is associated with the passage of a synoptic ridge. Seibert (1990) emphasizes that the warm air advection on the Alpine north side, building up the low-level cross-Alpine temperature differences, happens prior to the approach of the upstream trough. Therefore, *Shallow Foehn* is regarded the natural predecessor of *Deep Foehn*.

100 Güller (1977) describes a Foehn event, where the synoptic conditions neither led to southerlies nor weak winds above crest level, but a strong, northwesterly jet prevailed above the Alps. Such synoptic conditions are typically associated with eastward moving storms on the Swiss Plateau (see Supplement Fig. S1a for orientation), but not with the formation of Foehn in the respective valleys. During this event, the cross-Alpine pressure differences mainly built up due to a strong pressure drop on the Alpine north side, related to the rapid approach of a secondary cyclone towards Central Europe. Accordingly, Burri et al.

105 (1999) classifies this Foehn variety as a special type of pre-frontal Foehn, occurring ahead of warm fronts. On the other hand, as the southerly winds are restricted to below crest levels, it can also be classified as an extreme case of *Shallow Foehn* (Seibert, 1990; Sprenger and Schär, 2001). Gerstgrasser (2017) also mentions that this Foehn type (named 'Gueller Foehn' or, in this study, *Gegenstrom Foehn*) can be considered a special variety of *Shallow Foehn*. Yet, from a mechanistic point of view, the cross-Alpine pressure differences build up differently, and the associated synoptic conditions are strikingly different than for

110 *Shallow Foehn*. Overall, there is barely any literature available with respect to this Foehn type, and, to the authors knowledge, no climatological assessment has been done so far.

In the late 90s and early 2000s, research on the Alpine South Foehn culminated in the Mesoscale Alpine Programme (MAP; Bougeault et al., 2001). During MAP, two different foci with respect to Foehn were targeted: One focus of MAP was on the local-scale aspects of Foehn dynamics in the widely branched Rhine Valley (Drobinski et al., 2007). In alignment with the

115 earlier studies, a pronounced case-to-case variability was noticed, e.g. with respect to the presence and intensity of upstream orographic precipitation. For a detailed description of the synoptic conditions associated with Foehn events in the Rhine Valley during MAP, it is referred to Richner et al. (2006). Another focus of MAP concerned research along the Austrian Brenner transect (Mayr et al., 2007). There, the primary focus was to investigate *Shallow Foehn* as a type of gap flow, whereby the phenomenon was studied in the context of hydraulic theory. MAP publications usually define *Shallow Foehn* as a Foehn with

120 either westerlies or weak winds above crest level (e.g., Gohm and Mayr, 2004).

Recent publications continue to emphasize the contrasts between a 'Swiss' and an 'Austrian Foehn' type. This distinction is, at least to some extent, motivated by the fact that Austrian Foehn events are only accompanied by upstream precipitation in about 50% of the time, whereas Swiss Foehn events are more often associated with precipitation (Seibert, 1990; Steinacker, 2006; Würsch and Sprenger, 2015). By combining high-resolution modelling with online trajectories, Miltenberger et al. (2016)

125 compare the air mass origin and the thermodynamics of air parcels for a *Dry Foehn* and a *Moist Foehn* event in the Rhine Valley. Besides evident differences in the latent heating contributions to Foehn air warming, *Dry Foehn* air parcels also stem from considerably higher altitudes over the Po Valley compared to *Moist Foehn* air parcels, which, partly, ascend from near-surface levels to the Alpine crest. This contrast, as highlighted by the two case studies, also emerges from the climatological

study conducted by Würsch and Sprenger (2015): Using a reanalysis data set at 7 km horizontal grid spacing, they present the first climatology of backward trajectories for Swiss Foehn (Altdorf) and Austrian Foehn (Ellboegen). Altdorf trajectories tend to ascend more steeply, and are more frequently associated with precipitation. However, the study stresses that Austrian Foehn can likewise occur in Switzerland and vice versa. While the Foehn hours are grouped depending on the minimum altitude of the trajectories over the Po Valley, they refrain from an explicit characterisation of different Foehn types for Altdorf. All of the recent Alpine South Foehn studies (Würsch and Sprenger, 2015; Miltenberger et al., 2016; Jansing and Sprenger, 2022) invoke the Lagrangian perspective to highlight the complex upstream flow pattern. The low-level easterly flow over the Po Valley is usually decoupled from the southwesterlies aloft (see also Rotunno and Houze, 2007), which leads to the formation of distinct airstreams contributing to the Foehn flow. There are, to this point, no studies that link upwind airstreams to different Foehn types in a climatological context.

In essence, two centuries of Foehn research have illustrated that there exist different Alpine South Foehn types. These are oftentimes viewed as different, characteristic stages of a single event, but can just as well occur individually. Differences between 'Swiss Foehn' and 'Austrian Foehn' have been highlighted from a Eulerian and a Lagrangian perspective. Most of this literature is, however, focusing on individual case studies. No climatological investigation with respect to different Swiss Foehn types has been conducted so far. Here, we present the first such analysis for Foehn in Altdorf. The specific questions we address are:

1. Are the different Foehn types mentioned in the literature distinguishable in terms of the synoptic conditions?

2. How does the vertical structure of the atmosphere differ between the different Foehn types on the Alpine scale?

3. Where and from which altitude does the Foehn air originate?

4. What is the typical thermodynamic evolution of Foehn air parcels for the different Foehn types?

5. What is the meteorological impact of the different Foehn types at Altdorf?

In order to tackle these research questions, we make use of the operational forecasting system employed at MeteoSwiss, the Swiss Federal Office of Meteorology and Climatology. It allows us to investigate an extensive five-year period using analyses. The data set, including 3D meteorological fields for all Foehn hours in Altdorf, offers unprecedented opportunities to study mesoscale characteristics of South Foehn types in the Alps.

In the remainder of the paper, after having presented the main data sets and methodological approach (Section 2), the first two research questions are addressed by the means of an analysis-based Foehn classification scheme (Section 3) and a composite analysis of the synoptic and Alpine-scale conditions during the different Foehn types (Section 4). The Foehn air origin and thermodynamic evolution with respect to the different Foehn types are dissected using backward trajectories calculated for each of the 2'329 Foehn hours (Section 5). Afterwards, the local-scale impact at Altdorf is scrutinized using observations (Section 6). Finally, Section 7 discusses some aspects with respect to the existing literature and Section 8 summarizes the key results of the study.

2 Data and methods

2.1 Station measurements and Foehn index

On the one hand, station measurements of the MeteoSwiss automatic meteorological network are used to characterise the local meteorological conditions at Altdorf (Section 6). On the other hand, they serve to identify Foehn hours at Altdorf (Section 3) and all other sites listed in the Supplement (Table S1). The operational real-time identification of Foehn at MeteoSwiss sites is based on an objective Foehn index (Dürr, 2008). For the work presented here, data from an enhanced offline version of the Foehn index maintained by the Alpine Research Group Foehn Rhine Valley/Lake Constance (AGF; www.AGFoehn.org) is used. The most important differences between the enhanced and the operational Foehn index are:

- usage of Grand St. Bernard (2472 m AMSL, abbreviated as GSB) as the reference site at the main Alpine crest instead of Gütsch (2286 m AMSL), which is used as backup site in case of data outage

- extension of the Foehn index for *Dimmer Foehn* and *Gegenstrom Foehn*

- inclusion of Foehn probability F for comparison with numerical weather prediction (NWP) model data

Dimmer Foehn and *Gegenstrom Foehn* are identified by testing the station measurements for strong winds from the site-specific Foehn wind sector, which are either more humid or potentially colder than the site-specific Foehn thresholds for relative humidity and for the potential temperature difference to the Alpine main crest site, respectively (Dürr, 2008). *Dimmer Foehn* situations with northwesterly winds at Jungfraujoch (3582 m AMSL) are denominated as *Gegenstrom Foehn* in the enhanced Foehn index.

The Foehn probability F [%] of the enhanced Foehn index is calculated as follows:

$$F = 30 \left(\frac{(\theta_s - \theta_{\mathrm{GSB}}) - \Delta\theta_t}{\Delta\theta_m - \Delta\theta_t} \right) + 30 \left(\frac{ff_s}{ff_m} \right) + 40 \left(\frac{RH_t - RH_s}{RH_t - RH_m} \right), \tag{1}$$

where θ denotes the potential temperature [K], $\Delta\theta$ the potential temperature difference between the local and the Alpine crest site [K], ff the wind velocity [m s^{-1}] and RH the relative humidity [%]. s denotes the local Foehn site, t the site-specific Foehn index threshold and m the mode, i.e. the maximum of the unimodal distribution of the respective quantities during Foehn periods (see Dürr, 2008, for details). $F < 0\%$ is set to 0% and $F > 100\%$ to 100%.

For the study, the Foehn probability F, which is given in 10 min intervals, needs to be converted into a binary Foehn timeseries at hourly resolution. When the mean F within a symmetric interval of [-30 min,+30 min] is larger than or equal to 50%, the respective hour is considered a Foehn hour. The aggregation results in 2'329 Foehn hours during the considered time period (29 Oct 2015–29 Oct 2020).

2.2 COSMO analysis data

The Consortium for Small-scale Modeling (COSMO) mesoscale numerical model solves a non-hydrostatic formulation of the governing thermo-hydrodynamical equations of the atmosphere (Steppeler et al., 2003; Baldauf et al., 2011). Subgrid-scale
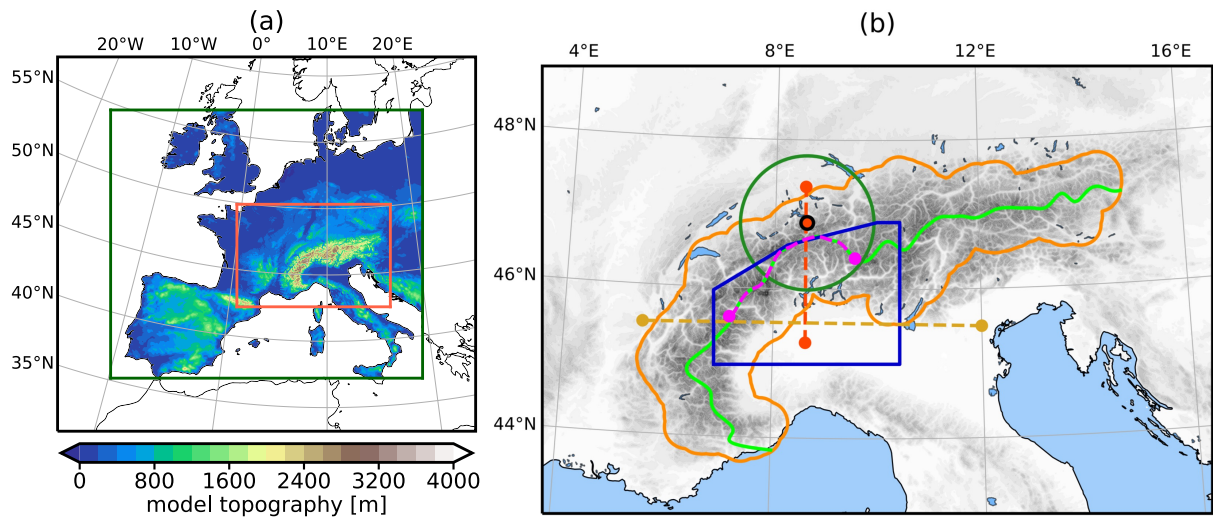
Figure 1. (a) Domains and topography of the COSMO-7 (green) and the COSMO-1 (red) analyses, respectively. (b) Polygon around the Alps and the crestline (dark orange and lime). Altdorf is highlighted by a red dot with a black edge. Further indicated are a circle for the wind feature extraction (green) and a polygon for the precipitation feature extraction (dark blue). The cross-Alpine cross section, the along-crest cross section and the upstream Po Valley cross section are marked as red, pink and golden dashed lines, respectively.

processes, including cloud microphysics, radiative transfer, turbulence and convection (for coarser resolution) are parametrized. Aside from a forecast model, the COSMO framework also comprises a data assimilation module. At MeteoSwiss, COSMO is used for operational forecasting at several resolutions and for generating atmospheric analyses. This study employs two analysis data sets from MeteoSwiss, namely COSMO-7 (6.6 km horizontal grid spacing) and COSMO-1 (1.1 km horizontal grid

195   spacing). The four-dimensional data assimilation in COSMO, as used for the time period considered, applies an observational nudging technique refined for complex terrain (Schraff, 1997). The assimilated data includes radiosoundings, aircraft and ship data, wind profiler and station measurements (surface pressure, 2-m dew point and wind below 100 m AMSL). Furthermore, radar data is assimilated using a latent heat nudging scheme (Stephan et al., 2008). The assimilation is performed in six-hourly and three-hourly cycles for COSMO-7 and COSMO-1, respectively. While COSMO-7 has been operational since the early

200   2000s, MeteoSwiss is operating COSMO-1 since March 2016 (pre-operational since autumn 2015). This enables us, for the first time, to systematically analyze and classify Foehn hours during five years on the Alpine scale.

For all the Foehn days which are identified (all days with at least one Foehn hour in the considered time period) and the days prior to allow for the calculation of backward trajectories, hourly 3D and surface fields are extracted from the MeteoSwiss archive for COSMO-1 and COSMO-7 analyses.

2.3 Trajectory calculations

Air parcel trajectories are frequently used in Foehn research to assess the origin and thermodynamic evolution of the Foehn air in various regions of the world (e.g., Elvidge and Renfrew, 2016; Kusaka et al., 2021), as well as the Alps (e.g., Würsch and Sprenger, 2015; Miltenberger et al., 2016; Saigger and Gohm, 2022). For the Lagrangian analysis based on COSMO-1 (Section 5), we calculate backward trajectories using the Lagrangian Analysis Tool LAGRANTO (Wernli and Davies, 1997; Sprenger and Wernli, 2015). Air parcels are released during each of the 2'329 Foehn hours and at every grid point within a 10 km circle around Altdorf (8.62°E / 46.89°N). The vertical distribution ranges from 20 m AGL up to 3 km with a vertical spacing of 100 m, which results in 4'241 trajectories for each Foehn hour and a total of 9'877'289 trajectories calculated. The internal time step for the integration of the trajectory equation is set to 5 min, while output is saved in 10 min intervals. Standard prognostic fields (temperature, pressure, wind components, specific humidity, five hydrometeor categories), as well as surface precipitation and the topography are traced along the trajectories.

While the analysis is inherently closer to observations compared to a freely running NWP model, a Foehn flow does not necessarily establish in COSMO-1 during each of the 2'329 Foehn hours and in the entire column of the valley atmosphere. To ensure that only trajectories arriving within a Foehn flow are considered for further analysis, air parcels need to fulfill two criteria: First of all, they need to be subject to a southerly wind at their time of release (wind direction between 90°–270°); secondly, they have to intersect the Alpine crestline (Fig. 1b). Together, these criteria reduce the sample size to 7'776'604 trajectories.

Offline trajectories calculated with hourly input wind fields can significantly deviate from online trajectories (Miltenberger et al., 2013) and offline trajectories with higher temporal input frequency (Schär et al., 2020; Saigger, 2021). This is especially true in regions where the flow is substantially distorted and highly transient owing to the complex terrain. Thus, we have to refrain from explicitly assessing the pathways of the air parcels from crest level into the Foehn valleys and from studying the mechanisms that lead to the descent. Instead, we assume the statistical distribution of trajectory positions at crest level to be reasonably well represented, and restrict our analysis to the trajectory segments upstream of their crest intersection (Fig. 1b). There, we are confident that the temporal resolution of the input fields from the NWP model suffices to study mean airstream properties.

3 Foehn classification scheme

Based on the available literature on different South Foehn types, we aim to distinguish between three main Foehn types related to distinctively different synoptic situations, and hence, crest-level flow conditions. The most typical situation, where the Foehn flow is accompanied by a deep layer of southerly or southwesterly winds (e.g., the first phase of Burri et al., 1999), is referred to as *Deep Foehn*. However, as elaborated in the introduction, Foehn can occur under strikingly different synoptic conditions. We separate between two additional main classes with either weak crest-level winds, i.e. weak synoptic forcing in the Alpine region (e.g. Gerstgrasser, 2017), or an eastward flow regime (e.g. Güller, 1977). These two types are denoted as *Shallow Foehn* and *Gegenstrom Foehn*, respectively. In previous literature, both weak winds and westerlies at crest level are frequently
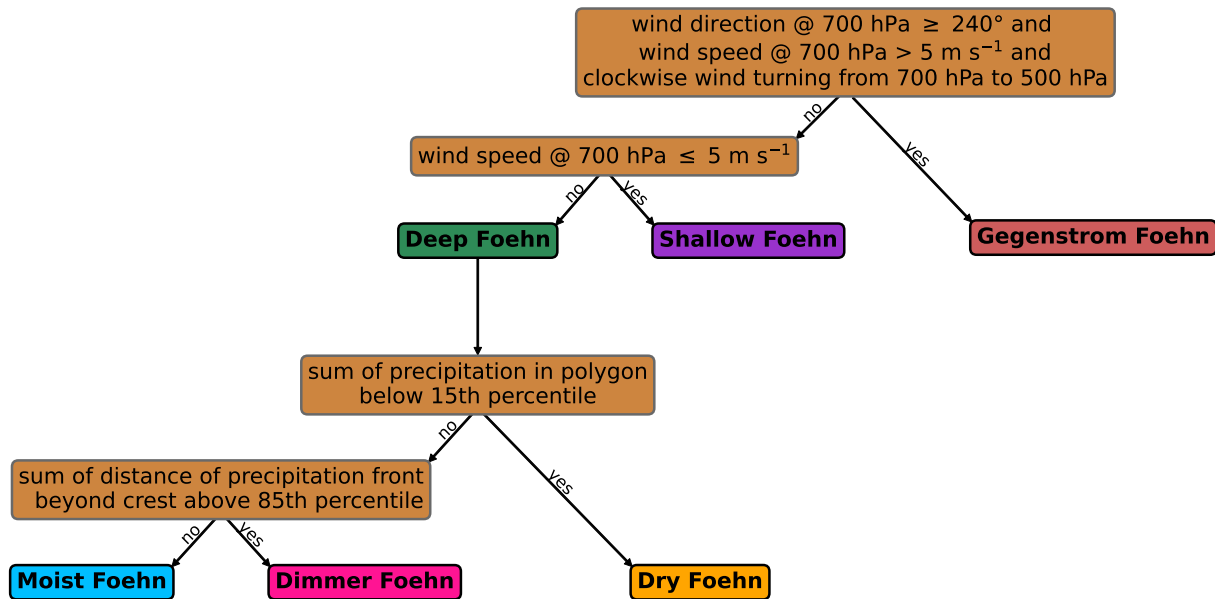
Figure 2. Sequential decision tree to classify the Foehn hours into three main Foehn types and three *Deep Foehn* subtypes.

summarized under the term *Shallow Foehn* (e.g. Gohm and Mayr, 2004). However, since the former two flow regimes are associated with considerably different synoptic situations over Central Europe, as will become evident in the following, we

240 differentiate between them and maintain the term *Shallow Foehn* for cases with weak crest-level winds. Accordingly, we label the zonal regime as *Gegenstrom Foehn*, a term introduced by the AGF (see Section 2.1).

The differentiation of the main Foehn types is done by following a sequential decision tree based on subjective thresholds for the wind direction and speed (Fig. 2). To this end, mean wind speed and direction in a circle with 100 km radius around Altdorf are extracted from the COSMO-1 analysis on 700 hPa and 500 hPa (see Fig. S2a in the Supplement for a distribution of these

245 quantities for all Foehn hours) in a region centered around Altdorf (green circle in Fig. 1b). Foehn hours with a rather zonal flow at crest level (wind direction between 240° and 360°, i.e. westsouthwest and north) of considerable magnitude (mean wind speed at 700 hPa exceeding 5 m s^{-1}) and an anticyclonic wind shear between 700 hPa and 500 hPa are labelled as *Gegenstrom Foehn*. Foehn hours with weak winds at crest level (mean wind speed at 700 hPa below or equal to 5 m s^{-1}) are categorized as *Shallow Foehn*, and the remainder is specified as *Deep Foehn*.

250 *Deep Foehn* can vary substantially with respect to the amount and extent of the accompanying orographic precipitation. In fact, it can occur without any precipitation on the southern side of the Alps (e.g., IOP1 of MAP with 0 mm precipitation in Lugano, as discussed in Drobinski et al., 2007). In stark contrast, other *Deep Foehn* events can be associated with intense upstream precipitation and, in some cases, the transient advection of precipitation beyond the Alpine crest into the northern Foehn regions. The latter is referred to as *Dimmer Foehn* (e.g, IOP2 of MAP according to Richner et al., 2006). Hence, it

255 is reasonable to further subdivide *Deep Foehn* according to the characteristics of the precipitation field (see Fig. S2b for a distribution of the quantities for the *Deep Foehn* subtypes). Extending the decision tree (Fig. 2) further, at first, the spatially

Table 1. Table providing the Foehn hours for the main Foehn types, their relative occurrence frequency and seasonality.

	All Foehn	Deep Foehn	Shallow Foehn	Gegenstrom Foehn
hours	2329 h	2080 h	147 h	102 h
fraction	100%	89.3%	6.3%	4.4%
DJF	19.8%	19.2%	0.0%	61.8%
MAM	48.4%	46.8%	87.1%	25.5%
JJA	5.1%	5.0%	4.8%	6.9%
SON	26.7%	29.0%	8.2%	5.9%

summed precipitation within a region (see dark blue polygon in Fig. 1b) extending from the Alps to the central and western Po Valley (see Fig. S1a for orientation) is extracted from the analysis. It is notable that, while few hours actually exhibit $0 \, \mathrm{kg \, h^{-1}}$ precipitation, the distribution of the accumulated precipitation is heavily long-tailed and the subjectively chosen threshold is
260   small compared to the median ($8.96 \times 10^9 \, \mathrm{kg \, h^{-1}}$). All Foehn hours below the 15th percentile of the precipitation distribution ($3.05 \times 10^8 \, \mathrm{kg \, h^{-1}}$), which are also categorized as *Deep Foehn*, belong to the *Dry Foehn* subtype. The remaining *Deep Foehn* hours are categorized with respect to the precipitation extent beyond the Alpine crest line. For an illustrative example the reader is referred to the Supplement (Fig. S3). The procedure is as follows: Within the crest segment bounded by the light blue circle in Fig. S3, the extent of the precipitation beyond the crest line is identified for each grid longitude by detecting the point north
265   of the crest line where the precipitation falls below $1 \times 10^{-6} \, \mathrm{mm \, h^{-1}}$ for the first time (light red line in Fig. S3). The resulting line is slightly smoothed (dark red line in Fig. S3) and the distance beyond the crest line is calculated for each point of the line. This distance metric is then summed up and all the cases where it exceeds the 85th percentile, and which are not categorized as yet, are labelled as *Dimmer Foehn*. The remaining Foehn hours are labelled *Moist Foehn*, corresponding to the archetypal *Deep Foehn* subtype.

270   In summary, this classification scheme results in three main Foehn types (*Deep Foehn*, *Shallow Foehn*, *Gegenstrom Foehn*) and three *Deep Foehn* subtypes (*Dry Foehn*, *Moist Foehn*, *Dimmer Foehn*). Their relative occurrence frequency compared to all Foehn hours and their seasonality are displayed in Tables 1 and 2. The overall Foehn hours and their seasonality approximately correspond to the climatological values as identified by Gutermann et al. (2012), whereas the overall Foehn frequency is slightly reduced ($466 \, \mathrm{h \, year^{-1}}$ compared to $483 \, \mathrm{h \, year^{-1}}$ for 1955–2008 in Gutermann et al., 2012). The correspondence indicates that
275   the five-year Foehn timeseries used in this study constitutes a time period that represents the climatological Foehn occurrence and seasonality in Altdorf reasonably well. The frequency of Alpine South Foehn peaks in spring and, to a smaller extent, in autumn, while a minimum occurs during summer. Note the pronounced inter-annual variability (Fig. S4), which aligns with earlier findings regarding the Foehn timeseries in Altdorf (Richner et al., 2014).

   Deep Foehn emerges as the most frequent Foehn subtype (89.3%) with a seasonality similar to the overall Foehn timeseries
280   except for a slight frequency shift from spring to autumn. 6.3% of all Foehn hours correspond to *Shallow Foehn*, most of which occur during spring. *Gegenstrom Foehn* is rare (4.4%) and mostly occurs during the winter months, when synoptic situations with a strong zonal pressure gradient over Central Europe develop more frequently. Using four years of station measurements

Table 2. Table providing the Foehn hours for the *Deep Foehn* subtypes, their relative occurrence frequency and seasonality.

	Dry Foehn	Moist Foehn	Dimmer Foehn
hours	312 h	1473 h	295 h
fraction	13.4%	63.2%	12.7%
DJF	11.2%	20.8%	19.7%
MAM	54.5%	45.5%	46.8%
JJA	10.6%	4.1%	3.7%
SON	23.7%	30.0%	29.8%

and radiosoundings, Seibert (1990) classified roughly 10% of all Foehn hours in Innsbruck (Austria) as shallow. Considering that they defined *Shallow Foehn* as a Foehn flow with both weak winds or westerlies above crest level, the frequencies for
285 *Shallow Foehn* and *Gegenstrom Foehn* in Altdorf are comparable to Innsbruck.

Focusing on the *Deep Foehn* subtypes (Table 2), the occurrence frequencies are evidently given by the percentile approach in the decision tree, which yields a frequency of 13.4% and 12.7% for *Dry Foehn* and *Dimmer Foehn*, respectively. *Dry Foehn* occurs more frequently during spring and summer, in contrast to *Moist Foehn* and *Dimmer Foehn*. To the authors' knowledge, there are, to this point, no studies specifically addressing the seasonality of *Dry Foehn* and *Dimmer Foehn*. Finally, *Moist*
290 *Foehn* as the main Deep Foehn subtype (63.2%), as well as *Dimmer Foehn* exhibit a seasonality comparable to the overall Foehn timeseries.

Additionally, the match of *Dimmer Foehn* and *Gegenstrom Foehn* hours as diagnosed with the decision tree are briefly compared to the corresponding Foehn types determined using station measurements (Section 2.1). In this regard, Table S2 summarizes the most important metrics of the comparison. During the five-year period, the Foehn index identifies both less
295 *Gegenstrom Foehn* and *Dimmer Foehn* hours compared to the classification using the decision tree. First of all, the Foehn index determines these types with the aid of point measurements, which differs from the approach in our study, that considers mean properties within certain regions (Fig. 1b and S3). Secondly, the station-based diagnosis of *Gegenstrom Foehn* applies more rigid thresholds for the wind field (northerly component at Jungfraujoch) and additionally includes relative humidity constraints, a criteria omitted by our classification. In summary, a certain discrepancy between the two classifications
300 is expected. However, when considering a time lag of 6 h, most of the station-based *Gegenstrom Foehn* and *Dimmer Foehn* hours are identically classified with the decision tree (87% and 75%, respectively; see Table S2), which, in fact, provides an observational-based validation for the classification.

4 Mean flow conditions during the Foehn types

4.1 Synoptic overview

305 To investigate the mean large-scale conditions during the different main Foehn types and *Deep Foehn* subtypes, composite fields on 500 hPa are calculated using the COSMO-7 analysis data. The main Foehn types are characterised by strikingly different synoptic conditions (Figs. 3a–c). During *Deep Foehn*, an upper-level trough is situated upstream of Switzerland with its center close to Ireland. Above Altdorf, southwesterlies of $14 \, \mathrm{m \, s^{-1}}$ prevail on 500 hPa (Fig. 3a). This flow configuration, usually accompanied by a surface low pressure system over the British Isles and its attendant cold front (not shown), is commonly

310 referred to as the characteristic synoptic situation inducing South Foehn in the Alps (e.g. Richner and Hächler, 2013). It corresponds to the trough Foehn category in Burri et al. (1999), although a pre-frontal Foehn can likewise be classified as *Deep Foehn*, since we do not distinguish between cases with a rapid frontal propagation (e.g., Hächler et al., 2011) and cases with a quasi-stationary cold front (e.g., Burri et al., 1999). In contrast, during *Shallow Foehn*, only a weak, but more elongated upstream upper-level trough is discernible. The Alps are situated in the col of a ridge over the Mediterranean and an anticyclone

315 over Northeast Europe, resulting in very weak synoptic forcing over Central Europe (wind speed of $0.5 \, \mathrm{m \, s^{-1}}$ above Altdorf) with a relatively high geopotential on 500 hPa (Fig. 3b). The Alps are approximately situated on the synoptic ridge line. The emerging synoptic situation is comparable to that described in Gerstgrasser (2017). In particular, weak easterlies can be observed over the Adriatic Sea and Northern Italy at 850 hPa (not shown). A similar situation can be observed during the first phase of the case study described in Mayr and Armi (2008), where the ageostrophic cold air advection around the eastern

320 edge of the Alps induces a cross-Alpine gradient in potential temperature and thus causes a shallow Foehn flow. *Gegenstrom Foehn*, in turn, is associated with strong westerlies ($25 \, \mathrm{m \, s^{-1}}$) and a pronounced geopotential height gradient over Central Europe (zonal flow regime; Fig. 3c). The large-scale situation with a veering of the wind from southwesterlies on 850 hPa to northwesterlies on 300 hPa (not shown) resembles the case study description of Güller (1977), albeit a more northerly flow on the jet level in his case study.

325 The subdivision of the *Deep Foehn* subtypes according to the precipitation field reveals that the longitudinal position of the upstream trough is different for each subtype (Figs. 3d–f). During *Dry Foehn*, the amplitude of the upstream geopotential disturbance is reduced and shifted northward. Instead, a ridge emerges over the southern Mediterranean with the synoptic ridge line shifted to the east of Switzerland. Wind speeds are slightly lower ($11.6 \, \mathrm{m \, s^{-1}}$) compared to *Deep Foehn* conditions. The synoptic situation during *Moist Foehn*, in turn, essentially resembles the *Deep Foehn* composite. This reflects the fact

330 that *Moist Foehn* constitutes the most important *Deep Foehn* subtype. During *Dimmer Foehn*, the trough is deeper and more elongated, which results in a synoptic trough axis closer to the Alps, lower geopotential height above Altdorf and stronger free-tropospheric southwesterlies of $18.5 \, \mathrm{m \, s^{-1}}$ on 500 hPa. While the *Deep Foehn* subtypes are distinguishable due to the varying trough position, they can also be envisioned as different stages of the same Foehn event, with a propagation and deepening of the upper-level trough when transitioning in the event's evolution from drier to moister phases.
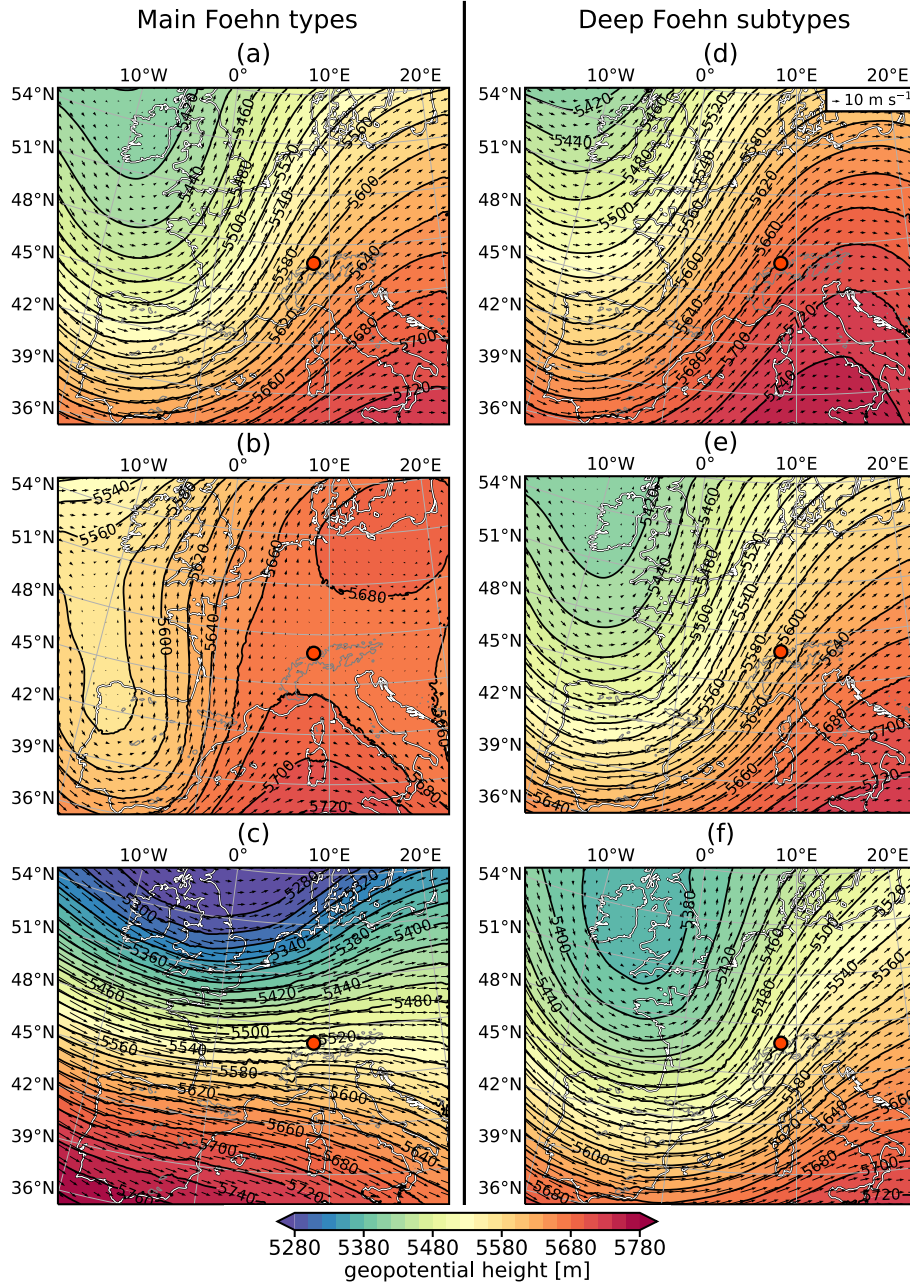
Figure 3. COSMO-7 composites of geopotential height (color and black contours) and horizontal wind field (vectors) at 500 hPa for the different main Foehn types and *Deep Foehn* subtypes. (a) *Deep Foehn*; (b) *Shallow Foehn*; (c) *Gegenstrom Foehn*; (d) *Dry Foehn*; (e) *Moist Foehn*; (f) *Dimmer Foehn*. Altdorf is marked as a red dot and the 1500 m contour of the Alps is indicated in grey.

4.2 Mesoscale structure across and along the Alpine crest

North-South cross sections with terrain-following streamlines and upstream precipitation have become a widespread illustration for cross-Alpine Foehn flows in many basic meteorological or high school textbooks (see Seibert, 2005, for a critical review of this development over time). This Section depicts composites of the vertical stratification, moisture distribution and cross-Alpine flow for the different Foehn types using the COSMO-1 analysis. In particular, the composite cross sections can be used to see how closely the different Foehn types correspond to the conceptual narrative shown in textbooks. In addition to north-south cross sections (in Fig. 4), west-east cross section composites along the Alpine crest will be shown (in Fig. 5).

During *Deep Foehn*, as discussed in Section 4.1 (Fig. 3a), southerly winds prevail in the mid-troposphere and down to levels below 2 km (not shown). As the southerly flow impinges on the Alps, the air is orographically lifted and, once it reaches saturation, clouds form, which is confirmed by the high relative humidity in the composite on the windward side of the Alpine barrier (Fig. 4a). Likewise, orographic precipitation forms upstream over the Po Valley and the southern side of the Alps with a mean intensity of approximately 1 mm h^{-1} (see Fig. S5a). Over the two highest peaks along the cross section, the atmospheric flow gets disturbed by the complex terrain. The deflection of the isentropes[1] indicates vertically propagating gravity waves. The southerly flow peaks in a layer above the crest at about 4 km over the western Swiss Alps and 3 km over the eastern Swiss Alps (Fig. 5a), while the wind speed maxima extend into the gaps of favorably oriented valleys (e.g., the Reuss Valley). In contrast, other valleys do not experience Foehn breakthrough (e.g., part of upper Rhine Valley region)[2]. Considering the isentropes in Fig. 4a as approximate streamlines, air parcels experience a strong descent immediately downstream of the crest associated with the vertically propagating mountain waves. The adiabatic compression leads to a warming of the air parcels and thus a decrease in relative humidity, a typical Foehn effect (see e.g. Richner and Hächler, 2013) clearly emerging along the cross section in the region around Altdorf.

During *Shallow Foehn*, the weak synoptic forcing leads to weaker orographic lifting without noteworthy upwind precipitation (see also Fig. S5b) and no gravity waves emanating from the mountain peaks along the cross section (Fig. 4b). The upstream stratification over the Po Valley differs substantially from the one during *Deep Foehn*: A weakly stratified mixed layer is capped by a strongly stratified layer at 3 km. Above, the free troposphere is relatively dry, as is typical for large-scale subsidence in anticyclonic weather regimes. However, downslope of the Alpine crest, the Foehn effect is apparent from reduced relative humidity. The along-crest composite (Fig. 5b) highlights the restriction of the Foehn flow to major Alpine south-north transects (gaps), primarily in Central and Eastern Switzerland, whereas calm conditions prevail above crest level. This confirms the findings from MAP describing *Shallow Foehn* along the Austrian Brenner transect as a type of gap flow (Mayr et al., 2007). Focusing again on the cross-Alpine vertical cross section (Fig. 4b), the potential temperature contours point to a temperature gradient across the Alps with colder temperatures on the Alpine south side (note that the same is also true for *Deep Foehn*). The

---

[1]In order to prevent artificial smoothing of isentropic deflections due to seasonal variations, potential temperature in Fig. 4 is shown with respect to a reference value. This is done by subtracting the mean potential temperature at 3 km altitude of each time step from the actual potential temperature field prior to compositing.

[2]Note that the crestline composite crosses the Valais (Fig. S1b) in its upper part, which, being oriented from the northeast to the southwest, often experiences weak northeasterly winds during Foehn.
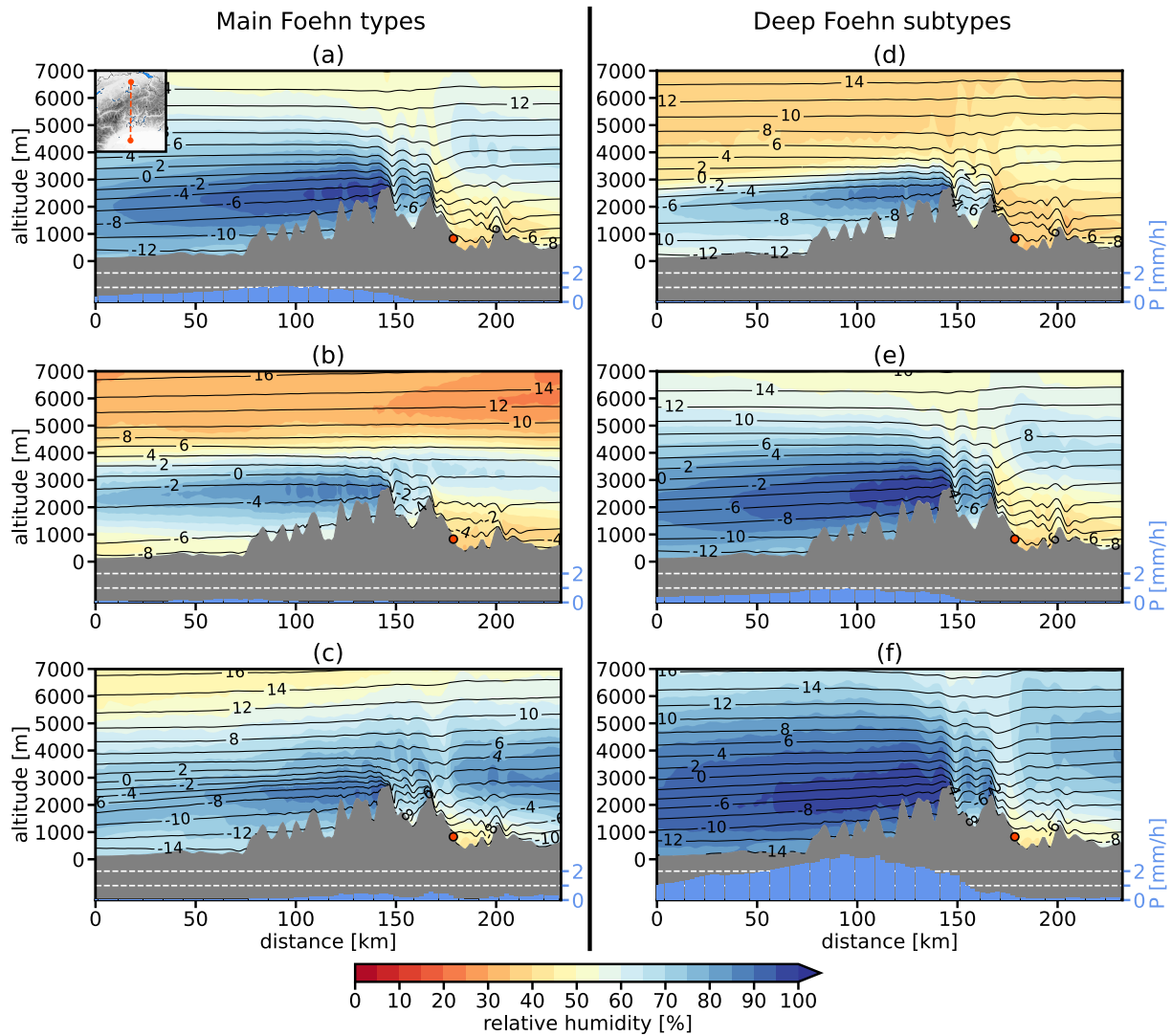
Figure 4. Alpine-crossing composites of relative humidity (color) and normalised potential temperature (black contours) in vertical cross sections based on the COSMO-1 analysis. Precipitation along the cross section is indicated as blue bars and the cross section path is displayed as a red line in the inset on the upper left of the first panel. (a) *Deep Foehn*; (b) *Shallow Foehn*; (c) *Gegenstrom Foehn*; (d) *Dry Foehn*; (e) *Moist Foehn*; (f) *Dimmer Foehn*. The latitudinal position closest to Altdorf is marked as a red dot.

temperature gradient is restricted to below-crest levels (< 3 km) and induces a hydrostatic pressure gradient across the Alps. As a result, *Shallow Foehn* develops as a hydraulic compensation flow driven by the temperature difference of the southern and northern air masses (Mayr and Armi, 2008). Consequently, *Shallow Foehn* can only develop where the gaps along the Alpine crest are low enough for the colder air mass to pass through. Hence, in Switzerland, the high Alps south of the Valais and the
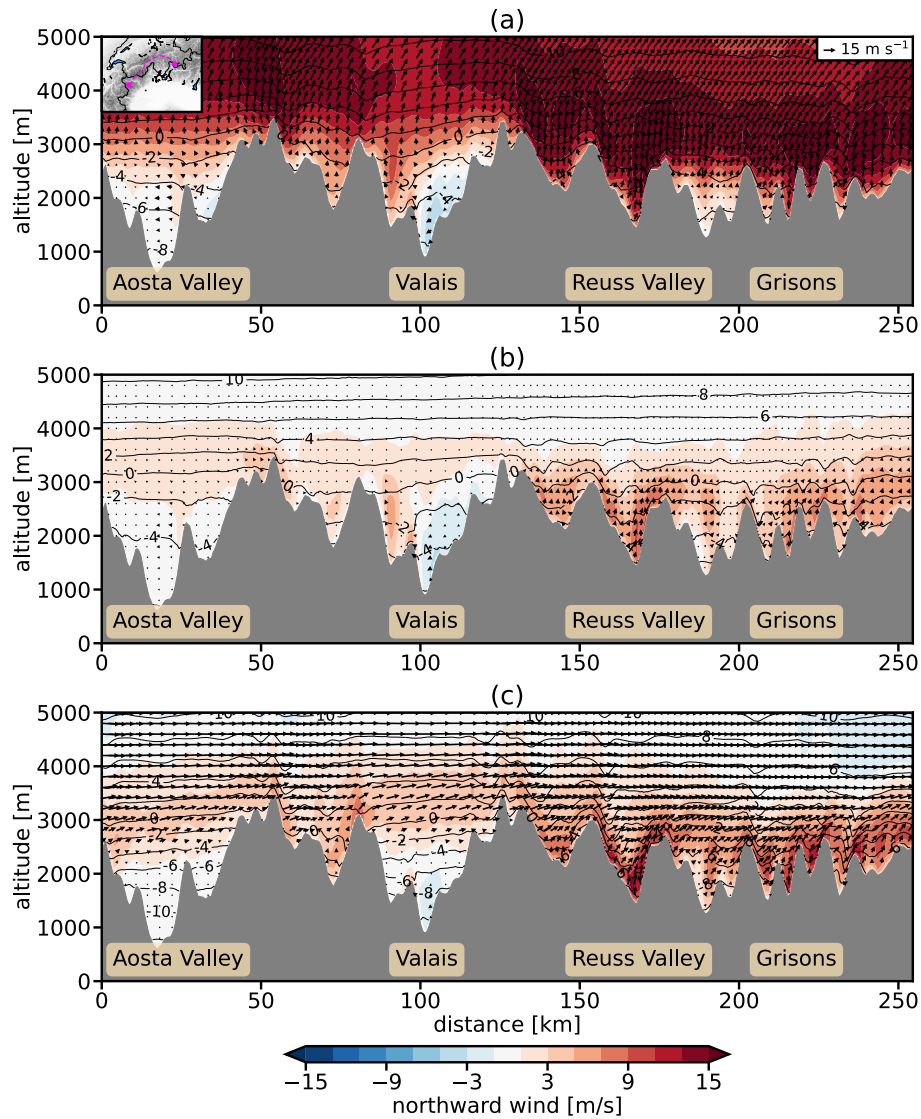
Figure 5. Same as Fig. 3 but along the crestline as defined in Section 2.2. The colors indicate the northward component of the wind and the arrows the horizontal wind field. Arrows pointing to the right correspond to eastward winds, arrows pointing upward to northward winds. Major gaps along the crestline are labelled. (a) *Deep Foehn*; (b) *Shallow Foehn*; (c) *Gegenstrom Foehn*.

Bernese Alps (Fig. S1b) largely inhibit the formation of *Shallow Foehn*, an effect also visible in composites of the horizontal
370 wind field at 2.5 km (not shown).

The zonal large-scale flow during *Gegenstrom Foehn* leads to a weak orographic lifting with little precipitation over the Alps as well as on the northern side of the Alpine rim (Figs. 4c and S5c). Still, moderate relative humidity values of air masses south and north of the Alps can be observed. On the Alpine south side, an even more pronounced stable layer, compared to

Shallow Foehn, is present at 2.5 km altitude. The downslope drying of the Foehn air is less pronounced, possibly owing to the
mixing with moist air masses advected with the westerlies north of the Alps. In accordance, Güller (1977) likewise describes
the relative humidity as abnormally high during such cases. The Foehn flow is again restricted to levels below 3 km, confining
it to major gaps along the Alpine transect (Fig. 5c). Above 3 km, a strong zonal flow prevails. In analogy to the *Shallow Foehn*
type, part of the driving cross-Alpine pressure gradient stems from the colder below-crest air mass on the Alpine south side.
However, the synoptic pressure gradient in a zone of enhanced baroclinicity across the Alps (see also the sloping of isentropes
above crest level in Fig. 4c) potentially further amplifies the cross-Alpine pressure gradient and thus favors the formation of a
Foehn flow.

The differences in depth and elongation of the upstream upper-level trough during the three *Deep Foehn* subtypes evidently
has an effect on the vertical distribution of moisture across the Alps (Figs. 4d–f). During *Dry Foehn*, the layer below the capping
inversion at 2.5–3 km only reaches moderate saturation levels (relative humidity 60–80%). The reduced upstream relative
humidity also affects the downstream relative humidity values in the Foehn region. Consequently, *Dry Foehn* emerges as the
Foehn type with the lowest relative humidity values in the northern Alpine valleys. With the stable layer over the Po Valley
capping the layer attaining moderate relative humidity levels underneath, and the low free-tropospheric relative humidity,
the mesoscale structure of *Dry Foehn* resembles the *Shallow Foehn* composite (compare Figs. 4b and 4d). Potentially, this
correspondence results from the upper-level ridge, which emerges during both of these types (see Figs. 3b and d). Again, *Moist
Foehn* largely corresponds to the *Deep Foehn* conditions previously described: The southerly flow induces orographic lifting
with upstream precipitation and vertically propagating gravity waves. *Dimmer Foehn*, on the other hand, emerges as a Foehn
variety accompanied by very intense orographic precipitation ($> 2 \, \mathrm{mm \, h^{-1}}$). As opposed to *Moist Foehn*, the atmosphere is
not only close to saturation at crest level, but the strong southwesterlies and, potentially, also large-scale lifting downstream
of the trough over the British Isles, induce elevated relative humidity values throughout the mid-troposphere. As typical for
Dimmer Foehn, the strong cross-Alpine flow leads to a partial spillover of precipitation into regions north of the main Alpine
crest (note precipitation north of the 150 km mark along the cross section). As a consequence, precipitation reaches the Foehn
region around Altdorf (see also Fig. S5f). Accordingly, the relative humidity in the lee-side valley air is higher than during
Moist Foehn, which is typical for *Dimmer Foehn* according to Richner and Hächler (2013).

In summary, the identified Foehn types with their distinct synoptic situations also differ with respect to their vertical structure
(relative humidity distribution, precipitation, stratification, flow field) along and across the Alps. To some extent, the mean *Deep
Foehn* conditions resemble the conceptual textbook model and the characteristics of the 'Swiss Foehn' type (Steinacker, 2006).
Nevertheless, the intensity of upstream orographic lifting and precipitation, as well as the presence and strength of a stable
layer at crest level, varies considerably for the different Foehn types. As a consequence, one can raise the question how these
differences are reflected in the origin and thermodynamic evolution of Foehn air parcels for the different Foehn types. To this
aim, the next Section will tackle these questions adopting the Lagrangian perspective.

5 Lagrangian analysis

Several recent studies point to the existence and varying importance of different airstreams contributing to Alpine Foehn events (Miltenberger et al., 2016; Jansing and Sprenger, 2022; Saigger and Gohm, 2022). These airstreams differ with respect to the horizontal and vertical origin of Foehn air parcels and the thermodynamic evolution along their transport pathway. In this Section we will investigate the extensive Foehn data set with respect to airstream occurrence, their air mass origin, and the thermodynamic evolution associated with them (Section 5.2). Furthermore, the linkage of upwind airstreams to the Foehn types and upstream stratification will be discussed (Section 5.3).

5.1 Trajectory classification

In order to analyze the occurrence of airstreams during Alpine South Foehn events in a systematic manner and to quantify their importance for the different Foehn types, backward trajectories are independently classified for the Foehn types. To this end, the changes of three positional variables (longitude: Δlon, latitude: Δlat, altitude: Δz) and three thermodynamic variables (temperature: ΔT, potential temperature: $\Delta\Theta$, specific humidity: ΔQV) with respect to the Alpine crest are extracted from the compiled trajectory data set (see Section 2.3 for details regarding the trajectory calculations). Specifically, the variables in the set are defined as the difference of the conditions at the Alpine crest relative to the conditions 6 h prior to crest arrival (e.g., Δlon = $\text{lon}_{\text{crest}} - \text{lon}_{\text{upstream}}$). Travel time is chosen instead of distance to crest, as some air parcels can deviate substantially from a linear north-south pathway, and hence remain close to the Alpine crest. Furthermore, the temporal threshold of 6 h ensures that changes, for example due to physical processes such as latent heating, are considered over a uniform time interval. When calculating backward trajectories using a limited-area model, air parcels eventually leave the domain at a certain time after being released. Thus, the reference time of 6 h is also chosen as a pragmatic threshold in order to include as many trajectories as possible for further analysis, while, at the same time, capturing the bulk of the upstream ascent for the majority of air parcels. With the chosen threshold, 279'036 trajectories, i.e. 2.8% of all trajectories, are excluded from further analysis since they leave the domain in less than 6 h after having crossed the defined crest line.

For further analysis, the variable set is standardized by subtracting the mean and dividing by the standard deviation for each of the variables. Then, the standardized variable set is used to perform a principal component analysis (PCA), which serves to reduce the dimensionality of the parameter phase space spanned by the six variables. The resulting biplot (Fig. 6) shows the first and second principal components (PC1 and PC2) and the projections of the original variables into the principal component space (vectors). The plot illustrates that the variability along the first principal component (PC1), explaining most of the variance (60%) in the six-dimensional phase space, is mainly governed by the thermodynamic variables and the altitude difference, which is expected to be strongly correlated with the thermodynamic evolution. Accordingly, variablity along the second principal component (PC2) is largely associated with horizontally varying trajectory positions relative to the crest (Δlon, Δlat). Since PC1 explains most of the variance, the trajectory data set is subdivided into terciles with respect to PC1 (see also the histogram with the chosen thresholds indicated as green, dashed lines in Fig. 6). Hence, trajectories with PC1 $\leq$ -0.83 belong to cluster 1, trajectories with -0.83 < PC1 $\leq$ 0.89 to cluster 2, and trajectories with PC1 > 0.89 to cluster 3.
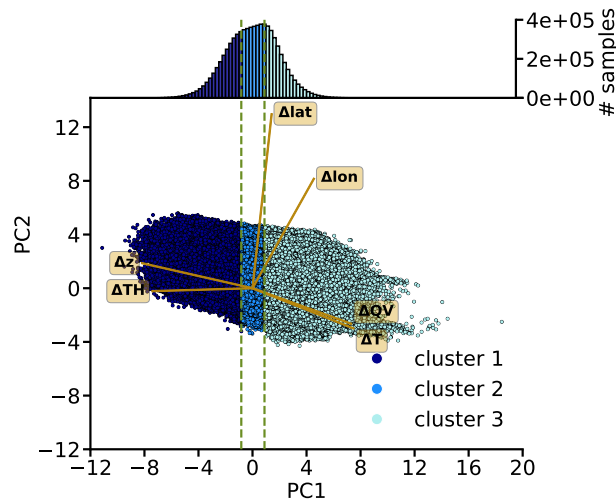
Figure 6. Biplot of PC1 and PC2 including the loadings (dark orange lines with labels in light brown boxes). The scores are colored in different shades of blue according to the three clusters based on PC1 terciles. A histogram of PC1 and the 33rd and 66th percentiles (green, dashed lines) are included as an inset above the biplot. For details on the PCA it is referred to the text.

5.2 Air mass origin and thermodynamics

440 As elaborated in the previous section, the trajectory clusters are defined based on PC1, whose variability is mainly governed by thermodynamic variables. However, the three clusters are also associated with a differing upstream origin of air parcels. This is also evident from the slope of the point cloud in Fig. 6. Trajectories in cluster 1 predominantly originate in the central to eastern Po Valley (Fig. 7a) at a median altitude of 1.5 km (Fig. 7b) and thus also ascend considerably while approaching the Alps. The origin of cluster 2 air parcels is shifted more to the west into the region of the Ligurian coast (see Fig. S1a for

445 orientation), as they only experience a slight deflection to the east relative to crest (Fig. 7a). They stem from a median altitude of 2.5 km, implying a slight ascent towards the crest (Fig. 7b). Finally, trajectories in cluster 3 are subject to the southwesterly flow above crest level and thus their origin is situated over the Maritime Alps (Fig. 7a). They exhibit a larger spread in their longitudinal position compared to cluster 1 and 2, which might be related to a corresponding variability in the Alpine-impinging synoptic flow. During their passage over the Western Alps and the northern Po Valley towards the main crest, they descend

450 from higher levels (> 3.5 km in the median; Fig. 7b). Trajectories in all three clusters reach the Alpine crest at a median altitude slightly lower than (cluster 1 and 2) or at 3 km (cluster 3). The different origin of the three trajectory clusters is linked to the characteristic directional shear pattern upstream of the Alps during Foehn events: Above crest-level, usually a southwesterly to southerly flow prevails (for *Deep Foehn*, see Fig. 3). Below crest, the flow is typically, at least partially, blocked by the Alps. The blocking effect leads to a westward flow deflection and the formation of an easterly barrier jet redirecting air parcels

455 towards the Alpine concavity in the region of Lago Maggiore (Schneidereit and Schär 2000; Medina and Houze 2003; Rotunno and Houze 2007). During heavy precipitation events with an enhanced low-level inflow of moisture, the combined effect of

the Coriolis force and the arc-shape of the Alpine barrier, is found to facilitate lifting in the western part of the Po Valley (Schneidereit and Schär, 2000), which potentially explains the considerable ascent of cluster 1 trajectories.

As vertical motion triggers cloud and precipitation formation, the three clusters are also characterised by a different diabatic transport history and varying precipitation intensity. To illustrate this, the thermodynamic evolution of the clusters is examined in T-Θ space (Fig. 8). This diagram is spanned by temperature on the x-axis, and potential temperature on the y-axis. Additionally, isobars are included to show the vertical evolution of the air parcels. Cluster 1 trajectories ascend most strongly (more than 150 hPa in the mean) during their approach to the Alpine crest, and therefore experience the most pronounced mean diabatic heating exceeding 4.5 K, as seen in the Θ-change. At the same time, corresponding to the moist adiabatic lapse rate of ~6 K km^{-1}, the moist-adiabatic ascent decreases temperature by 11.5 K. The mean pathway in T-Θ space points to pronounced latent heating during cloud formation. Cluster 2 air parcels are subject to a weak, nearly adiabatic ascent of 25 hPa during the first 3 h. Overall, they experience a moderate diabatic heating of ~1 K in the mean. As both cluster 1 and 2 approach the Alpine crest, their ascent speed increases. Note that their mean trajectory in T-Θ space reveals that they start descending (increase in temperature and pressure) prior to the crest arrival, defined as intersection with the crestline (lime line in Fig. 7a). This is likely caused by the fact that the smoothed crestline in the region of Altdorf extends slightly further north than the highest peaks in this region. Furthermore, the phase line of vertically propagating gravity waves usually tilt upstream (Smith, 1979), which might induce a descent of air parcels even before they have reached the crest. However, the descent appears during a minor segment of the trajectories and, hence, should not affect the main findings.

Cluster 3 is associated with a contrasting thermodynamic evolution compared to the other two clusters. From 6 h until 2 h prior to arrival, the air parcels descend at an almost constant temperature in the mean. This indicates that the mean adiabatic heating during the descent is compensated by an accompanying mean diabatic cooling of ~1.5 K. As the descent accelerates, mainly during the last hour prior to crest arrival, the trajectories experience a mean warming of ~3.5 K, while they are subject to further diabatic cooling of ~2.5 K. At the crest, cluster 3 trajectories are still at a slightly higher level compared to cluster 1 and 2.

The unique air mass origin and diabatic evolution of the three trajectory clusters can be linked to their upstream humidity changes and surface precipitation (Fig. 9). For this assessment, binned trajectory maps are constructed as follows: All trajectory increments starting from 6 h prior to their arrival are binned onto a regular 0.04° x 0.04° rotated latitude longitude grid (equator at 43° N, zero meridian at 10° E). Within each bin and for each cluster, mean properties are then calculated. Bins with less than 1000 trajectories are masked to enhance visibility and ensure that only representative areas are displayed (see masked area in Fig. S6). Air parcels of cluster 1 lose more than 2.5 g kg^{-1} of moisture and are associated with widespread precipitation exceeding 0.5 mm h^{-1} (Fig. 9a). Thererfore, cluster 1 emerges as the main precipitating Foehn airstream. Two main regions of strong moisture loss and precipitation can be identifed. Inflow from the central to eastern Po Valley produces precipitation along the southern flanks of the Alps and south of the Lago Maggiore region. Besides, a secondary inflow (less trajectories in cluster 1 originate from this region; see Fig. S6a) from the Mediterranean is related to a pronounced decrease in humidity and precipitation along the Ligurian coast and the Maritime Alps. The humidity loss corroborates that the potential temperature increase is induced by irreversible moist-adiabatic ascent and precipitation formation along the trajectories. Combined with
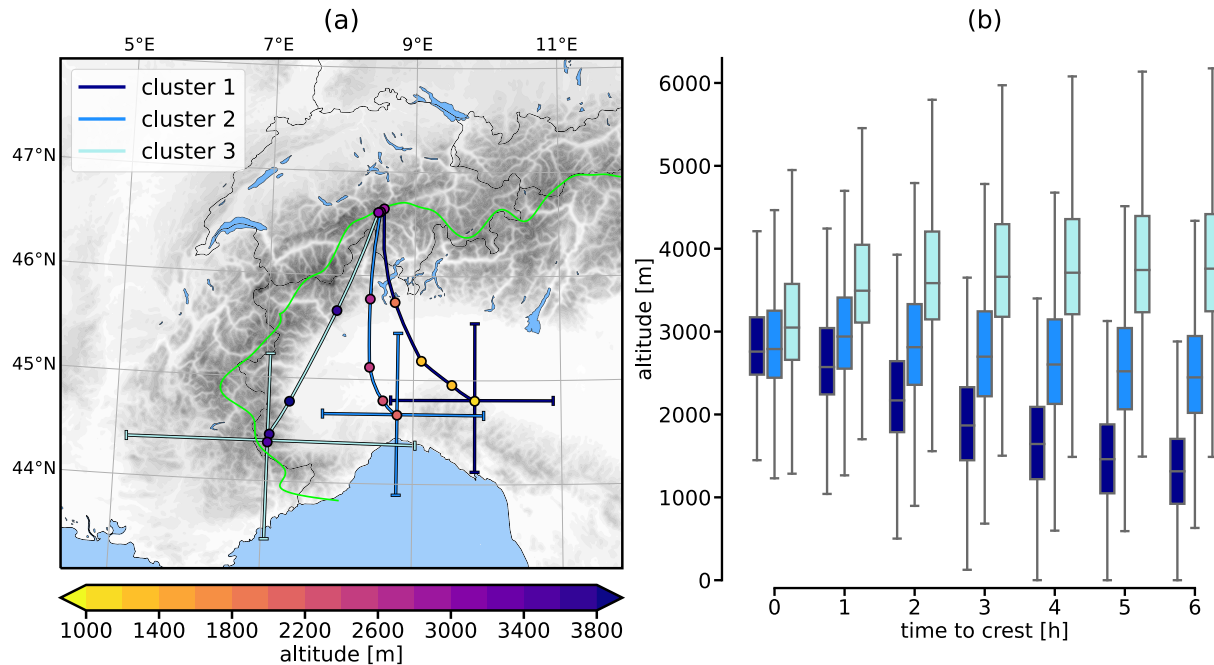
Figure 7. (a) Mean pathways of the three trajectory clusters (bold lines in shades of blue) and variability of the position 12 h prior to arrival at the crest (bars ranging from minus to plus one standard deviation in longitudinal and latitudinal direction, respectively). Dots mark every three hours and are colored according to the mean altitude of the clusters at the respective time step. Note that for the data points earlier than 6 h with respect to crest, the mean is calculated by excluding trajectories that left the domain in the meantime. (b) Height distribution of the three trajectory clusters starting from 6 h prior to crest in hourly intervals. The boxplots whiskers range from 1.5 times the interquartile range below the first quartile to 1.5 times above the third quartile, respectively. Outliers are not shown.

its pronounced diabatic heating and the strong upstream ascent, this cluster corresponds to the classical 'Swiss Foehn' type (Steinacker, 2006; Würsch and Sprenger, 2015).

As opposed to cluster 1, the specific humidity of trajectories from cluster 2 only decreases slightly ($-0.5 \, \mathrm{g \, kg^{-1}}$) and mainly
495   when air parcels originate at the Ligurian coast (see also mean pathway in Fig. 7a). The nearly saturated air mass is confined to the Lago Maggiore area (not shown). Therefore, cluster 2 is associated with minor amounts of precipitation.

Finally, and even more so than cluster 2, the trajectories of cluster 3 do not produce precipitation. In contrast, they gain humidity along their pathway towards the crest ($0.5 \, \mathrm{g \, kg^{-1}}$). The moisture gain could either be induced by evaporation of cloud and rain droplets, or result from entrainment of more humid air from below by vertical turbulent mixing. Likewise, both of
500   these processes (evaporation, turbulent mixing), or radiative cooling, could be responsible for the diabatic cooling observed along cluster 3 air parcels (Fig. 7b). The mean cloud water content along the trajectories increases as well (not shown). This renders evaporation unlikely to govern most of the diabatic cooling and points towards entrainment driving the moisture gain. However, enhanced mixing would require a weak stratification, which, in turn, makes strong cooling along the descending
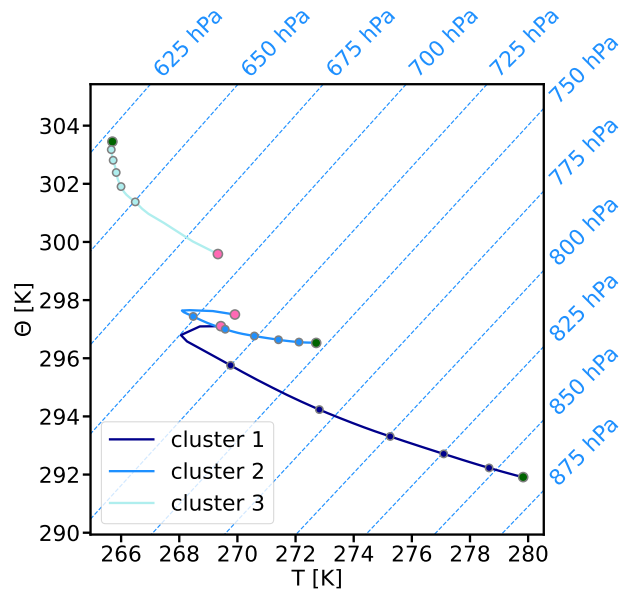
Figure 8. Thermodynamic evolution of the mean of each cluster in T-Θ space from 6 h before arrival at crest (green dot) to crest (pink dot). Dots mark each hour and isobars are displayed as blue dashed lines with a spacing of 25 hPa.

trajectories more unlikely. Overall, it remains unclear which diabatic process drives the cooling along cluster 3 trajectories and induces the moisture gain.

5.3 Linkage of trajectory clusters to Foehn types

Section 4 revealed substantial differences between the different Foehn types with respect to the intensity of upstream moist processes. Hence, the aim of this Section is to link the Foehn types to the occurrence of the different trajectory clusters that potentially induce these differences. The *Deep Foehn* subtypes will be analysed concurrently with the remaining main Foehn types, since *Deep Foehn* is dominated by the *Moist Foehn* subtype and therefore tends to show the same characteristics as the latter.

At first, it is unravelled how the three trajectory clusters contribute to the different Foehn types. In this regard, the *Deep Foehn* subtypes exhibit particularly pronounced differences (Fig. 10). *Dry Foehn* trajectories mainly belong to clusters 2 and 3, which implies that the air parcels originate from elevated upwind levels and do not experience significant latent heating and no upstream precipitation. A shift in the relative contributions can be observed for *Moist Foehn*, where the contribution of cluster 1 becomes more relevant, resulting in approximately equal contributions of all clusters. This clearly links to the terrain-forced lifting, condensation and orographic precipitation formation as derived from the composite analysis in Section 4.2 (Fig. 4e). For *Dimmer Foehn*, in turn, cluster 1 trajectories are dominant. The latter is in alignment with the Eulerian analysis conducted, where *Dimmer Foehn* emerges as associated with intense and widespread orographic precipitation (Figs. 4f and S5f). *Shallow Foehn* and *Gegenstrom Foehn*, on the other hand, are not related to considerable upstream precipitation (Figs. 4b and c), which
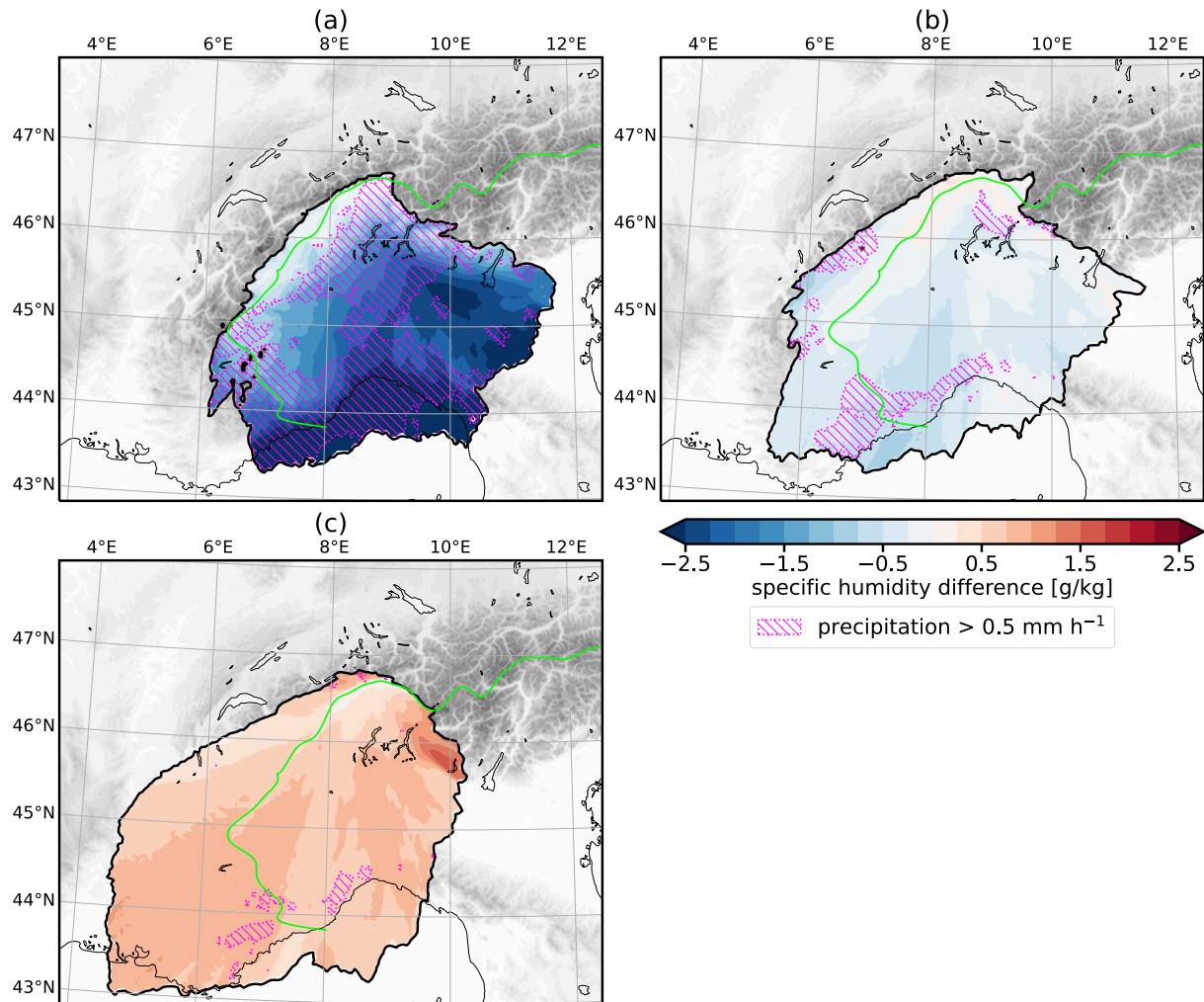
Figure 9. Binned trajectory maps with specific humidity changes relative to crest (in color) and precipitation exceeding $0.5\,\mathrm{mm\,h^{-1}}$ (as dashed violet areas) for the different trajectory clusters: (a) cluster 1; (b) cluster 2; (c) cluster 3. Areas with less than 1000 trajectory positions contributing to the mean are masked. See Fig. S6 for density maps depicting the number of trajectories within each bin. The crestline is indicated as a lime line.

results in a fairly small contribution from cluster 1 trajectories. Cluster 2 and 3 equally contribute to *Shallow Foehn*. Cluster 3, which originates from the southernmost tip of the Alpine arc, constitutes the governing airstream during *Gegenstrom Foehn*, since the large-scale flow above crest level has a pronounced westerly component during *Gegenstrom Foehn*.

The sourcing of Foehn air parcels is linked to the upstream stability as already described by Elvidge et al. (2015) for the Antarctic peninsula. To disentangle this relationship, the vertical stability of the different Foehn types is revisited in combination with the main upstream source altitude of the three trajectory clusters. The zonally oriented cross sections in Fig. 11 are colored according to the mean frequency by which the squared Brunt–Väisälä frequency ($N^2 = g/\Theta * d\Theta/dz$) exceeds
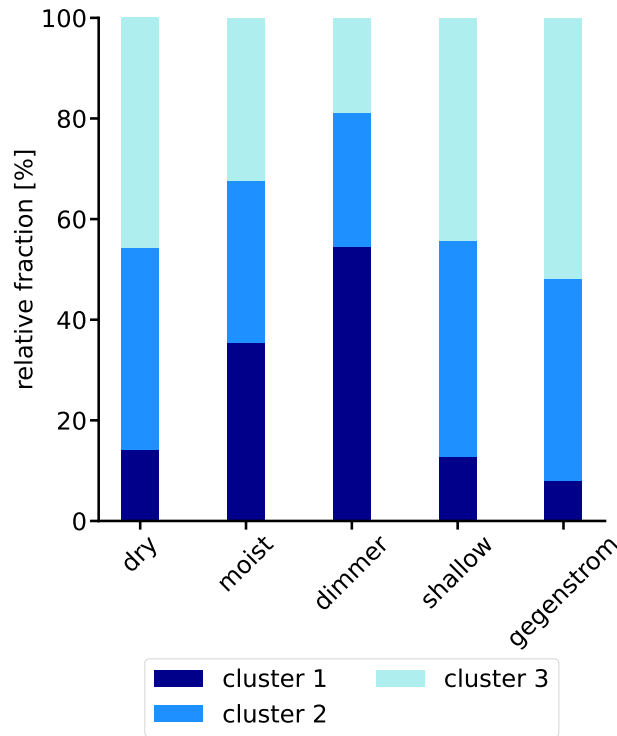
Figure 10. Relative contributions of the different trajectory clusters to the overall trajectory sample for the different Foehn types.

$2\times10^{-4}\,\mathrm{s}^{-2}$. Altitudes with a higher frequency of exceedance correspond to regions of high static stability and indicate the po-tential presence of an inversion layer. Besides, the composites also show favourite horizontal and vertical locations where the
530 Foehn air parcels intersect the cross section. To this end, the intersection location of each parcel is extracted and binned along the cross section on a 100 m x 50 m grid in the horizontal and vertical, respectively. The resulting density field is normalized to the total number of trajectory intersections for each Foehn type to allow for a comparison between the different types.

Dry Foehn is associated with the frequent presence of a stable layer at 2.5–3.5 km. This stably layer tends to be higher in the Western Alps compared to the Eastern Alps (Fig. 11a). Air parcels, mainly belonging to clusters 2 and 3, either approach
535 the Alps at the top of the stable layer over the Piedmont Alps (cluster 3) or within the layer and at its lower boundary over the eastern Po Valley (cluster 2). The levels below 2 km contribute little to *Dry Foehn* (cluster 1), indicating the potential role of the stable layer that largely inhibits the ascent of air parcels from lower levels. During *Moist Foehn*, elevated frequencies of N^2 exceedance occur at the same altitude as for *Dry Foehn*, but the values are significantly reduced (Fig. 11b). As a consequence, the ascent of low-level air parcels is facilitated. The hot-spots of trajectory intersections thus shift from the above-crest level
540 to 2.5 km (cluster 2) and 1.5 km in the eastern to central Po Valley (cluster 1). The stability structure of *Dimmer Foehn*, as indicated by the frequency pattern, essentially corresponds to the one observed during *Moist Foehn* (Fig. 11c). Cluster 1 is dominant during *Dimmer Foehn*, which is why its density is elevated in a widespread region at an altitude of 1.5 km in the central Po Valley. Interestingly, the isentropes indicate a low-level (below 2 km) zonal temperature gradient in the Po Valley
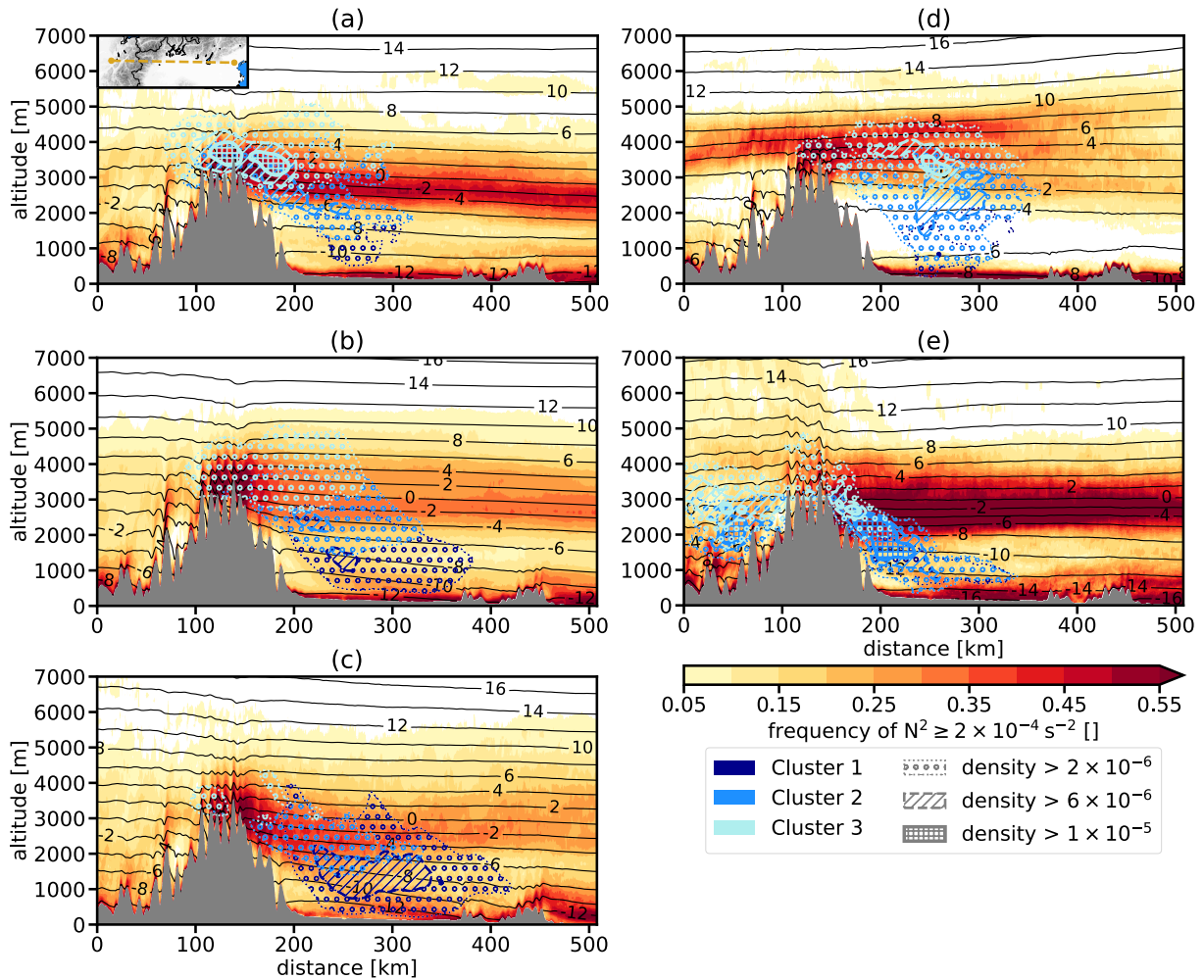
Figure 11. Frequency of N^2 being equal to or exceeding $2 \times 10^{-4}\,\mathrm{s}^{-2}$ in east-west oriented vertical cross section composites. Trajectory intersections for the three clusters (different shades of blue) are binned along the cross section and displayed as hatched contours (density $> 2 \times 10^{-6}$ with circles, $> 6 \times 10^{-6}$ with lines, $> 1 \times 10^{-5}$ with squares). Normalised potential temperature is displayed (black contours) as in Fig. 4. (a) *Dry Foehn*; (b) *Moist Foehn*; (c) *Dimmer Foehn*; (d) *Shallow Foehn*; (e) *Gegenstrom Foehn*.

during both *Moist Foehn* and *Dimmer Foehn* (Figs. 11b and c). As cluster 1 is associated with the easterlies of the Po Valley barrier jet (see also Section 5.2), isentropic upglide might additionally support the low-level ascent of air parcels during moist Foehn events.

Shallow Foehn is associated with a stable layer above crest level (3.5–4.5 km) in the western Po Valley and extending over the Western Alps (Fig. 11d). The majority of cluster 3 air parcels approach the Alps from above 3 km and, thus, in the lower part of the stable layer. Cluster 2 trajectories, on the other hand, intersect the cross section well below the stable layer. In fact, some air parcels even originate from near-surface levels. The lowermost part of the atmosphere over the Po Valley is weakly

stratified, as already described in Section 4.2 (Fig. 4b). The weak stratification indicates that the Po Valley boundary layer is usually well-mixed during *Shallow Foehn*. As a result, the boundary layer mixing feeds some air parcel into the main airflow crossing the Alps through major gaps. The downward extent of the trajectory densities illustrates that a first-order estimation of the altitude of origin, purely based on the presence of a stable layer, might be misleading.

555   *Gegenstrom Foehn* is characterised by the most pronounced stable layer of all Foehn types (Fig. 11e), which extends over the entire Po Valley in an altitude range between 2.5–3.5 km. In contrast to the other Foehn types, a considerable fraction of cluster 3 and cluster 2 trajectories approach the Alps from the most southwestern tip of the Alpine arc. The strong southwesterlies prevailing during *Gegenstrom Foehn* might support the lifting of these air parcels along the western flank of the Alps. A second hot-spot of trajectories can be found in the Piedmont Alps along the eastern flank of the Alpine arc. Trajectories originate at

560 levels down to below 1.5 km despite the pronounced stable layer above. Either, these air parcels reach just the lower limit of the stable layer and cross the Alps through the major north-south gaps (see Fig. 5), or they are subject to pronounced mechanical lifting despite the strong stratification. Furthermore, the northward slope of isentropes during *Gegenstrom Foehn* (Fig. 4c) indicates adiabatic ascent as air parcels approach the crest.

    In summary, the Lagrangian analysis reveals a different air mass origin and altitude for each of the thermodynamically

565 defined trajectory clusters. The air parcels originating more to the east generally ascend from lower levels, while the trajectories originating from above crest-level are advected with the southwesterly large-scale flow. The diabatic heating is more pronounced for trajectories associated with stronger upstream ascent, which confirms the presence of latent heating in clouds for these air parcels. Cluster 1 trajectories are associated with a pronounced moisture loss and widespread precipitation. Hence, this cluster is mainly relevant during *Moist Foehn* and *Dimmer Foehn*, while cluster 2 and 3 are more important for *Dry Foehn*,

570 *Shallow Foehn* and *Gegenstrom Foehn*. The upstream stratification is found to partially govern the altitude from where air parcels approach the Alps. However, additional processes play a role as well (e.g., turbulent mixing) and it becomes clear that the strength of the upstream stable layer alone cannot be considered an unambiguous predictor of the source altitude for Foehn air parcels.

6   Impact of Foehn types in Altdorf

575 The previous Sections 4 and 5 focused on an in-depth investigation of Eulerian and Lagrangian characteristics of the different Alpine South Foehn types on the mesoscale. This last results Section complements the analysis by examining the local meteorological impact of the Foehn types at Altdorf in the Reuss Valley (see red dot in Fig. 1b). This is of special interest to forecasters, who aim at an accurate prediction of local surface conditions, e.g., in Foehn valleys. In this context, it is valuable to know the characteristic conditions at Altdorf related to a certain Foehn type as diagnosed by the synoptic conditions. To this

580 end, station measurements at Altorf are grouped according to the prevailing Foehn type (Fig. 12).

    The *Deep Foehn* subtypes do not exhibit significant differences with respect to the observed wind speed and gusts (Figs. 12a and b). All the subtypes are associated with mean winds ranging from approximately 10–65 km h^{-1} and a median slightly below 40 km h^{-1}. Likewise, the gusts range from 15–105 km h^{-1} and exhibit a median of ~60 km h^{-1}. The degree of similarity

with respect to the flow conditions is, on the one hand, surprising, as the large-scale flow gets continuously stronger for the moister subtypes (*Moist Foehn* and *Dimmer Foehn*) compared to *Dry Foehn*. In agreement, the cross-Alpine pressure difference between Lugano (a station on the Alpine south side) and Kloten (on the Alpine north side) tends be largest for *Dimmer Foehn* and smallest for *Dry Foehn* (see Fig. S7 in Supplement depicting pressure differences between Lugano and Kloten for the different Foehn types). However, all of the *Deep Foehn* subtypes are prone to gravity wave activity, which might account for the observed similarities in wind speeds and gusts (compare the medians and boxes of the three *Deep Foehn* subtypes). Furthermore, precipitation spillover during *Dimmer Foehn* increases the stability of the valley atmosphere. Potentially, this weakens the Foehn penetration close to the Alpine crest and acts to reduce surface wind speeds despite the stronger cross-Alpine pressure difference (see also Zängl, 2006).

Shallow Foehn emerges as considerably weaker (mean winds of 10–30 km h^{-1}, gusts of 20–55 km h^{-1}) compared to the other Foehn types. This matches with the along-crest composites (Fig. 5b), where *Shallow Foehn* also manifests as the Foehn type with the weakest cross-Alpine flow. During *Shallow Foehn*, the cross-Alpine pressure gradient is primarily of hydrostatic nature due to the colder air mass on the Alpine south side. Hence, it is less pronounced than during the other Foehn types (Fig. S7). Potentially, the absence of gravity wave activity (see Section 4.2) acts to further reduce wind speeds within the Foehn valley.

Gegenstrom Foehn exhibits slightly reduced mean winds and gusts compared to the *Deep Foehn* subtpyes, but is, at the same time, considerably stronger compared to *Shallow Foehn*. Mean wind speeds range from 5 km h^{-1} up to 65 km h^{-1} with a median of 32 km h^{-1}, while the gusts range from 20–100 km h^{-1}. The stronger winds and gusts can, again, be explained considering the cross-Alpine pressure gradient (Fig. S7). During *Gegenstrom Foehn*, the gradient is of comparable magnitude as for the *Deep Foehn* subtypes with the overall largest median difference (~8 hPa). The pressure gradient during *Gegenstrom Foehn* can be additionally amplified owing to two reasons. First of all, a pronounced synoptic pressure gradient is superimposed to the hydrostatic pressure gradient generated by the low-level temperature differences (see Fig. 3c). Secondly, *Gegenstrom Foehn* events are oftentimes characterised by the passage of secondary storm lows, e.g., over northern Germany (Güller, 1977; Gerstgrasser, 2017). When such disturbances approach Central Europe, they induce a rapid pressure drop on the Alpine north side. Potentially, this leads to the stronger, more gusty characteristic of *Gegenstrom Foehn* in comparison to *Shallow Foehn*.

The dryness of Foehn winds is heavily invoked as one of their archetypcal characteristics (e.g., Richner and Hächler, 2013). Considering the relative humidity of the different Foehn types, however, a pronounced variability can be observed (Fig. 12c). The overall lowest values in relative humidity are reached for *Dry Foehn* (17–40 %; median at 30%). The large-scale subsidence during *Dry Foehn* inhibits precipitation, and sometimes even cloud formation upwind of the Alpine range (Gerstgrasser, 2017). The free troposphere above the stable layer at crest level, constituting the main source region for air parcels of this *Deep Foehn* subtype (Fig. 11a), is typically associated with low relative humidity values (Fig. 4d). As a consequence, unusually low relative humidity values compared to *Moist Foehn* can also be observed in the lee-side Foehn valleys. The observed relative humidity values tend to be larger for the moister *Deep Foehn* subtypes. The median of *Moist Foehn* and *Dimmer Foehn* amount to 34% and 39%, respectively. Strikingly, the distribution of *Dimmer Foehn* is heavily long-tailed towards higher values. The partial spillover of precipitation onto the leeward side increases relative humidity values of the precipitating air in cases when it reaches Altdorf. Elevated relative humidity values compared to *Moist Foehn* are a typical characteristic of *Dimmer Foehn*
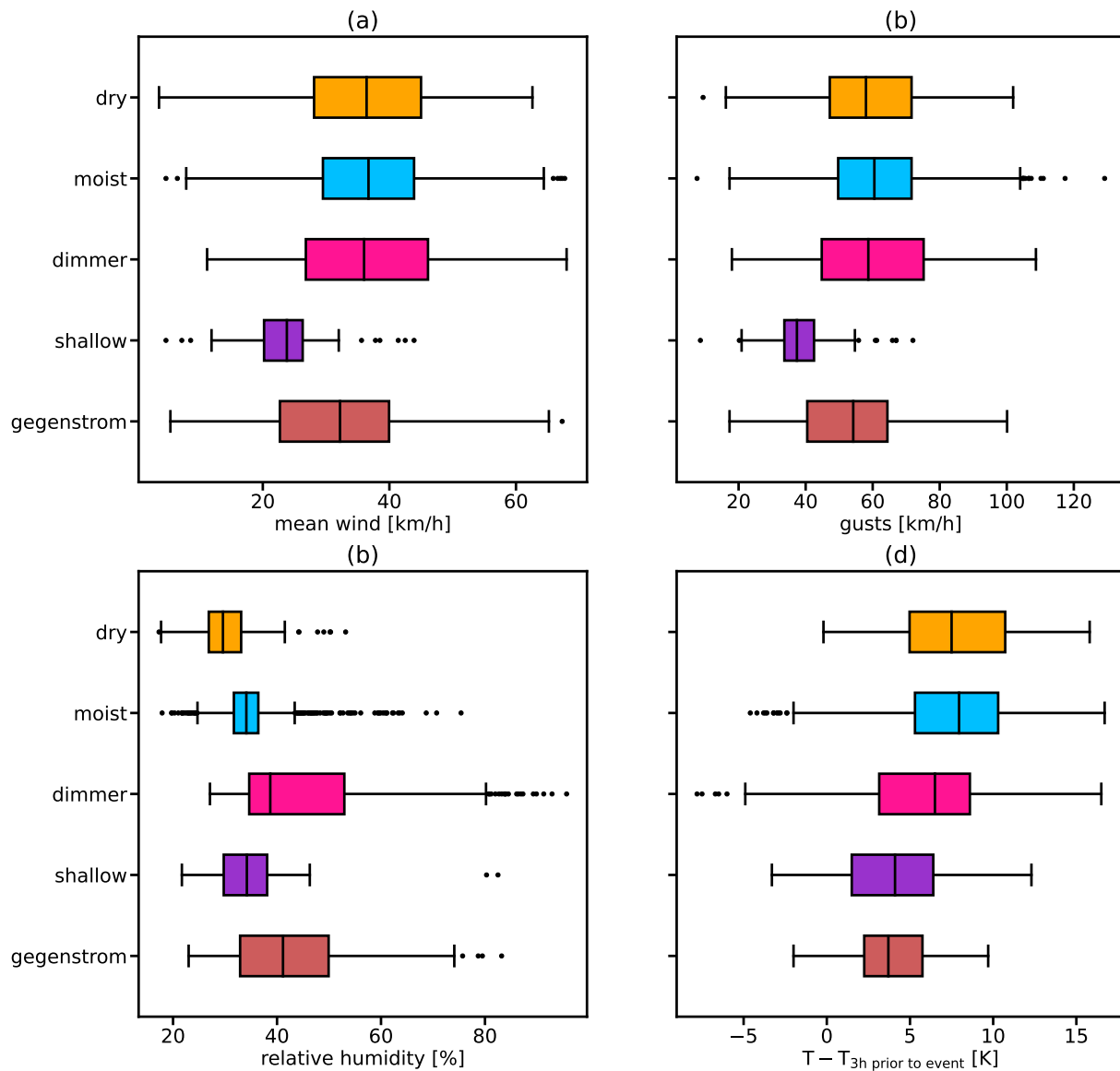
Figure 12. Boxplots of Altdorf station measurements of (a) mean wind speed, (b) wind gusts, (c) relative humidity and (d) the temperature difference for the different Foehn types.

(Richner and Hächler, 2013). *Shallow Foehn* is associated with similar relative humidity values as *Moist Foehn*, ranging from
620 20 to 45%. *Gegenstrom Foehn*, on the other hand, likewise tends to be associated with elevated relative humidity compared to *Moist Foehn*. In contrast to *Dimmer Foehn*, the moister air mass does not result from a partial spillover over the crest, but rather from the mixing of the drier Foehn air with the moist zonal flow north of the Alps (see also Fig. S5c for the precipitation composite of *Gegenstrom Foehn*).

Additionally, the temperature increase at the station owing to the Foehn breakthrough is compared for the different Foehn types (Fig. 12d). It is quantified by subtracting the temperature 3 h prior to Foehn onset from the instantaneous temperature during Foehn. To define the time of Foehn onset, the 2329 Foehn hours are grouped into continuous Foehn events, where an event is defined as a consecutive occurrence of Foehn hours with a maximum Foehn pause of 3 h (resulting in 168 events). This simple approach neglects the influence of the daily cycle on temperature differences, which is, however, strongly dampened during Foehn in Altdorf. For an example timeseries of temperature in Altdorf during Foehn, the reader is referred to Richner and Hächler (2013). The warming is strongest for *Dry Foehn* and *Moist Foehn*, for which the median amounts to 7.5 K and 8 K, respectively. The temperature differences exhibit a considerable spread ranging from below-zero values to values exceeding 15 K. Outliers on both sides of the distribution for the different Foehn types are most probably related to either an influence of the daily cycle, or a rapid air mass change during Foehn breakdown. *Dimmer Foehn* is associated with a less pronounced temperature increase than the other *Deep Foehn* subtypes (median of 6.5 K). This could be explained by considering the thermodynamic history of *Dimmer Foehn* air parcels. As precipitation falls into the sub-saturated atmosphere of the Foehn valleys, rain evaporation induces lee-side diabatic cooling. The cooling counteracts the adiabatic warming induced by the descent and leads to an overall reduced warming. The magnitude of the warming is further lowered during *Shallow Foehn* (~4 K). A potential explanation considers the gap flow characteristics of such events. As air parcels only cross the Alpine crest through major gaps, they are not able to gain as much elevation difference as if descending from crest level during *Deep Foehn*, hence the Foehn air warming due to isentropic drawdown is reduced. However, systematically assessing the penetration pathways of *Shallow Foehn* air parcels is beyond the scope of this study and could only be accomplished using online trajectories (e.g., Jansing and Sprenger, 2022) or offline trajectories calculated with a much higher temporal input frequency of the 3D wind fields (e.g., Saigger and Gohm, 2022). Finally, *Gegenstrom Foehn* is also characterised by a reduced warming of ~4 K. Similar potential mechanisms might reduce the warming effect, again including a reduced descent of air parcels or evaporative cooling downstream of the Alpine crest. Güller (1977) already quantifies the temperature difference of the Foehn air and the non-Foehn westerlies to be 4 K during his case study. *Gegenstrom Foehn* is also known as a rather 'cold' Foehn type among forecasters. However, the temperature difference at Altdorf not only depends upon the characteristics of the Foehn air, but is also influenced by the temperature structure of the pre-Foehn valley atmosphere. Hence, systematic differences in the pre-Foehn conditions between the different Foehn types (e.g, a more frequent presence of cold-air pools during one particular Foehn type) likely also play a role for the magnitude of the observed temperature difference. Further, more process-based investigations would be beneficial to improve the understanding of these differences in the Foehn air warming for the different Foehn types.

Overall, the investigation of the local-scale impact revealed pronounced differences between the different Foehn types. The *Deep Foehn* subtypes and *Gegenstrom Foehn* are associated with stronger winds compared to *Shallow Foehn*. This is presumably, at least partly, governed by differences in the cross-Alpine pressure gradient. The characteristic dryness of the Foehn wind at Altdorf varies, too. Relative humidity values are likely to be influenced by the recent thermodynamic history of the air arriving within at the valley floor. The same is also true for the temperature increase at the station, which is however also

influenced by the pre-Foehn valley conditions. In cases, where precipitation is advected over the Alpine crest (*Dimmer Foehn*) or with the upper-level westerlies (*Gegenstrom Foehn*), below-cloud rain evaporation acts to cool and moisten the Foehn air.

7 Discussion

7.1 The classification in a historical context

The Foehn classification presented in this study builds upon the long record of research on the Alpine South Foehn. The body of literature comprises an extensive list of different Foehn types, including, for example, 'anticyclonic Foehn', 'cyclonic Foehn', 'dimmerfoehn', or 'shallow Foehn'. In this regard, several aspects are discussed in order to highlight similarities as well as discrepancies of our Foehn types to the existing literature.

First of all, Foehn onset can occur while the Alpine region is still under the influence of an anticyclone and subsidence prevails above an elevated inversion layer. But does our *Dry Foehn* subtype correspond to the 'anticylonic Foehn'? An answer to this question is not straightforward, not least because the definition of the latter is rather vague in the literature. Billwiller, according to Kuhn (1984), considered the large-scale subsidence during this initial stage as a type of Foehn wind, a view rightfully challenged by Gubser (2006). At the same time, 'anticyclonic Foehn' is also described as a Foehn where geopotential above the Alps is higher than usual, the isohypses are curved anticyclonically, and the Alpine south side completely lacks precipitation. Sometimes, even cloud-free conditions prevail (e.g., Burri et al., 1999; Gerstgrasser, 2017). This characteristic of 'anticyclonic Foehn' is also shared with our *Dry Foehn*. Another analogy can be drawn with respect to the 'Austrian Foehn' type, which occurs in absence of upstream precipitation, yet blocked cold air decouples the Po Valley boundary layer from the southerly flow aloft (Steinacker, 2006). Again, *Dry Foehn* characteristics, as elaborated in Section 4, match with the 'Austrian Foehn' type. Analogously, the main 'cyclonic stage' of a typical Foehn event according to Billwiller, relates to our *Moist Foehn* subtype. During 'cyclonic Foehn' or the 'stationary stage' (Ficker, 1910), upstream orogaphic precipitation frequently forms and a Foehn wall establishes along the main Alpine crest (Frey, 1992). Likewise, the 'Swiss Foehn' type corresponds to our *Moist Foehn* and *Dimmer Foehn* subtypes, and to the 'trough Foehn' category of Burri et al. (1999). The mean synoptic conditions during *Dimmer Foehn* confirm several properties emerging from case studies in the literature (e.g., Streiff-Becker, 1947), as for example the low-pressure system being closer to the Alps, and stronger crest-level winds. However, diagnosing *Dimmer Foehn* from NWP data poses a particular challenge, since it is a local lee-side phenomenon. Hence, our classification should not be over-interpreted, as its definition is based on the overall spillover of precipitation beyond the crest in the Central Alps, rather than the actual presence of *Dimmer Foehn* within the Reuss Valley at Altdorf. Finally, it is notable that the different *Deep Foehn* subtypes (*Dry Foehn*, *Moist Foehn*, *Dimmer Foehn*) are oftentimes considered different stages during the typical temporal evolution of a Foehn event (e.g., Ficker, 1910; Streiff-Becker, 1933). Our subtypes resemble, to some extent, these stages ('anticyclonic Foehn', 'cyclonic Foehn', 'dimmerfoehn'), as described for example by Streiff-Becker (see Kuhn, 1984). However, as the study classifies Foehn hours instead of Foehn events, it remains to be investigated how often the subtypes transition from one to the other within the same event.

690   The occurrence frequency of *Shallow Foehn* (6.3%) is comparable to the value reported in Seibert (1990) for the Austrian Brenner transect (10%). Furthermore, the analysis confirms the gap flow characteristics of *Shallow Foehn* as analysed during MAP (Mayr et al., 2007). The gap flow is driven by a colder air on the Alpine south side, inducing a northward hydrostatic pressure gradient force (Mayr and Armi, 2008). A rather puzzling finding concerns the weakly stratified boundary layer over the Po Valley during *Shallow Foehn*. This outcome contrasts earlier results from MAP, where *Shallow Foehn* events were

695   usually associated with enhanced upstream stability (see e.g., Mayr et al., 2004). However, when comparing our results to MAP literature, some caution is required. MAP studies defined *Shallow Foehn* as a Foehn flow occurring while calm winds *or* westerlies prevailed above crest level, whereas the latter would often be classified as *Gegenstrom Foehn* using our classification scheme. Besides, the reduced stratification might also be an effect of seasonality rather than a property related to the Foehn type itself. During the analysis period of five years, *Shallow Foehn* predominantly occured during spring (87.1%). At the same

700   time, Würsch and Sprenger (2015) detected a relatively weak upstream stratification over the Po Valley for Foehn in Altdorf during spring. Whether the weak stratification links to the *Shallow Foehn* type or the seasonality could be addressed in a future study using a longer timeseries.

    As mentioned in the introduction, *Gegenstrom Foehn* could also be regarded as a special type of *Shallow Foehn* (e.g., Seibert, 1990). However, due to the strikingly different synoptic conditions, i.e. very strong and zonal large-scale flow, we consider it

705   justified to define a separate category for such events. Furthermore, additional processes, besides north-south temperature differences, might magnify the pressure gradient during this Foehn type. This includes the rapid pressure drop related to an approaching cyclone on the Alpine north side (Güller, 1977), and the pronounced synoptic pressure gradient. While the enhanced north-south pressure difference identified in Section 6 corroborates this hypothesis, more process-based studies would certainly be beneficial to better understand this exceptionally rare Foehn type.

710 ## 7.2   Lagrangian characteristics of the Foehn types

Recent studies on the Alpine Foehn frequently apply Lagrangian diagnostics to study the evolution of air parcels prior to their arrival in the northern Foehn valleys (Würsch and Sprenger, 2015; Miltenberger et al., 2016; Saigger and Gohm, 2022; Jansing and Sprenger, 2022). In this context, a few aspects of our Lagrangian analysis are discussed and an outlook to potential future studies is given.

715   On the one hand, air parcels during *Dry Foehn* originate from higher elevations upwind, which matches the first studied case of Miltenberger et al. (2016) and supports isentropic drawdown to be the main Foehn air warming mechanism for this *Deep Foehn* subtype. However, air parcels during *Moist Foehn* and *Dimmer Foehn* originate from significantly lower levels. This, on the other hand, is consistent with the thermodynamic theory according to Hann (1866), where Foehn air parcels are diabatically heated during their upstream ascent towards the Alpine crest. Overall, in agreement with Jansing and Sprenger

720   (2022), the variability in the upstream ascent points towards a more balanced view on Foehn air warming, where different mechanisms can govern the Foehn-induced temperature increase, depending on the event. Besides, even for a certain subtype (e.g., *Moist Foehn*), trajectories can originate from various levels upwind, and not all of them ascend steeply towards the crest. Thererfore, a detailed heat budget analysis for a multitude of Foehn events and types needs to be conducted in order to increase

the certainty with respect to the findings of Section 5. Besides, the trajectory analysis can be re-linked to a question posed in Seibert (1990) with respect to the fate of the low-level easterlies in the western Po Valley. With our analysis, we reveal that a part of this easterly flow actually ascends to contribute to the flow in Altdorf during *Moist Foehn* and *Dimmer Foehn*. A future study will revisit the lifting mechanism that provides these air parcels the ability to ascend from the boundary layer. Especially, it will be of interest whether the presence of a low-level temperature gradient in the Po Valley can facilitate the lifting via isentropic upglide.

In comparison to Würsch and Sprenger (2015), besides *Dry Foehn*, also *Shallow Foehn* exhibits 'Austrian Foehn' characteristics. More precisely, this means air parcels stem from an elevated source region, lose little to no moisture during their approach to the Alpine crest, and are associated with negligible amounts of precipitation. Furthermore, all of the Foehn types not (or only weakly) associated with precipitation (*Dry Foehn*, *Shallow Foehn*, *Gegenstrom Foehn*) exhibit a pronounced stable layer at approximately crest level, which confirms the description of Seibert (1990) for a typical 'Austrian Foehn' event. At the same time, *Moist Foehn* and *Dimmer Foehn* correspond to the 'Swiss Foehn' type. This, however, illustrates that the 'Swiss Foehn' category of Würsch and Sprenger (2015) contains events with strikingly different characteristics. Hence, it needs to be stressed that not even both, but multiple Foehn types can occur at the same location depending on the driving synoptic conditions. To some extent, this has already been confirmed by Würsch and Sprenger (2015) with regard to the large spread in the upstream properties (e.g., altitude) of air parcels as identified by their Lagrangian analysis.

Some of the findings with respect to the Lagrangian analysis cannot be entirely explained by our study. First of all, it seems that the very pronounced stable layer near crest level constitutes a less decisive factor for the vertical sourcing of air during *Gegenstrom Foehn*. It remains, however, unclear what the lifting mechanisms are in such cases. The authors can only speculate upon the potential role of the western flank of the Western Alps and the pronounced north-south baroclinicity across the Alps. Further investigations are needed to understand the mechanisms acting to lift air parcels during such cases.

Additionally, the study is not able to fully explain the observed humidity increase and diabatic cooling diagnosed along cluster 3 trajectories. Diabatic cooling can be caused by different processes (evaporation, mixing, longwave cooling), and explicitly determining their importance would require temperature tendencies along the trajectories (as in Jansing and Sprenger, 2022). Interestingly, Miltenberger et al. (2016) found slightly increasing humidity values upstream of the crest in their *Dry Foehn* case as well, which, at least, provides additional confidence in the diagnosed humidity trend. However, for a more in-depth study of the turbulent mixing process inducing the moisture gain, Lagrangian particle dispersion models would be better suited compared to kinematic air parcel trajectories used in this study. The same likewise holds true for a more exact quantification of the input of air parcels from the Po Valley mixed layer below the strongly stratified layer during *Shallow Foehn*. A final remark regarding cluster 3 trajectories concerns their travel over more complex terrain compared to the other clusters. As a result, the accuracy of these trajectories might be reduced compared to cluster 1 and 2 air parcels, which mainly travel over the Po Valley (see also Section 2.3).

8   Conclusions

This study aims at formalising different types of Alpine South Foehn mentioned in the literature, as well as characterising them from the synoptic to the Alpine scale. Furthermore, emphasis is given to their local meteorological impact at Altdorf, a location within a major Swiss Foehn valley on the Alpine north side. To this end, we employ an observational-based Foehn index to define a Foehn timeseries for Altdorf. The timeseries, covering five years of Foehn occurrence (Nov 2015–Nov 2020), accumulates to a total of 2'329 Foehn hours that are analysed with the aid of operational COSMO analyses. The high resolution of the analysis data (1.1 km spatial and 1 h temporal) allows us to scrutinize the mean conditions of the different Foehn types on the Alpine scale as well as to investigate the origin of the air and the upstream thermodynamics from a Lagrangian point of view. The key results are summarized as follows:

- A subjective decision tree serves to classify each Foehn hour as one of three main Foehn types (*Deep Foehn*, *Shallow Foehn*, *Gegenstrom Foehn*) and, if belonging to the *Deep Foehn* type, three respective subtypes (*Dry Foehn*, *Moist Foehn*, *Dimmer Foehn*). The main Foehn types are associated with strongly contrasting synoptic conditions. While *Deep Foehn* occurs downstream of an upper-level trough, *Shallow Foehn* is related to calm winds above crest level (weak synoptic forcing). *Gegenstrom Foehn* occurs during strong zonal large-scale flow within a region of pronounced synoptic pressure gradients over Europe. The *Deep Foehn* subtypes, in turn, differ with respect to the elongation and depth of the upstream upper-level trough. A more eastward trough axis and a deeper trough tends to induce stronger and more widespread upstream precipitation with spillover beyond the Alpine crest.

- The differences in the synoptic conditions are also reflected in contrasting mesoscale conditions across the Alps. A deep layer of southwesterlies impinging on the Alpine barrier during *Deep Foehn* induces orographic lifting and precipitation on the upwind side. No noteworthy orographic effect except flow channelling is present during *Shallow Foehn*. The colder air on the south side of the Alps induces Foehn as a hydraulic compensation flow (i.e., a gap flow) between the two air masses on both sides of the Alps. For *Gegenstrom Foehn*, the northward component of the flow is confined to the major Alpine north-south gaps as well. Above crest level, strong zonal winds advect moist air masses from the west. Among the *Deep Foehn* subtypes, *Dry Foehn* emerges as the one associated with dry conditions above crest level, potentially related to anticyclonic subsidence. While the conditions during *Moist Foehn* largely resemble the *Deep Foehn* type, intense orographic precipitation is observed upwind of the Alps during *Dimmer Foehn*. Partial spillover of precipitation into the usually dry Foehn regions on the north side is diagnosed.

- Lagrangian backward trajectories, calculated for each of the Foehn hours, are classified into three clusters using a PCA-based metric. The three resulting clusters are linked to a different air mass origin and, accordingly, a distinct mean thermodynamic evolution. Cluster 1 trajectories originate over the central to eastern Po Valley at a mean altitude of 1.5 km. Hence, they ascend considerably during their anticyclonically curved approach to the Alpine crest (at 3 km altitude), experience pronounced latent heating in clouds ($\Delta\Theta$ ~4.5 K), and constitute the main precipitating airstream of Foehn air parcels arriving in Altdorf. Trajectories in cluster 2 originate at the Ligurian coast at a mean altitude of 2.5 km.

Hence, they experience weaker latent heating ($\Delta\Theta$ ~1 K) as compared to cluster 1 trajectories during their slight ascent and, therefore, cluster 2 is associated with little precipitation. The characteristics of cluster 3 strongly contrast those of the other two clusters: Originating from above crest level (3.5 km), the air parcels are advected with the southwesterly large-scale flow towards the crest upstream of Altdorf. These air parcels descend towards Alpine crest level, are subject to a diabatic cooling of 4 K, and a slight moisture gain.

– As cluster 1 is the main precipitating airstream, it is especially important for *Moist Foehn* and *Dimmer Foehn*. Clusters 2 and 3, on the other hand, are more important for *Dry Foehn*, *Shallow Foehn* and *Gegenstrom Foehn*. The upstream stability profile is found to partially govern the vertical sourcing of Foehn air parcels. A pronounced stable layer confines most of the Foehn air parcels to originate from regions above 2.5 km during *Dry Foehn*, as it largely inhibits ascent from the Po Valley boundary layer. During *Moist Foehn* and *Dimmer Foehn*, where the stable layer is much less pronounced, more air parcels are able to ascend from levels below 2 km, i.e. cluster 1 becomes more prominent. The upstream stable layer during *Shallow Foehn* again limits the origin of most cluster 3 trajectories to above 3 km altitude. However, in contrast to *Dry Foehn*, cluster 2 trajectories partially originate from lower levels. This might be induced by upward mixing within the weakly stratified boundary layer in the Po Valley. While a very pronounced stable layer is present during *Gegenstrom Foehn*, it appears to be less decisive for the vertical origin of the Foehn air parcels. Potential reasons include the fact that a major part of the air parcels originates on the western flanks of the Western Alps, and the pronounced northward slope of isentropes during *Gegenstrom Foehn*, which supports isentropic upglide during the approach of the crest from the south.

– The presence of different Foehn types exhibits a profound impact on the local conditions at Altdorf as diagnosed by station measurements. While the mean wind and the gusts are of similar magnitude for the *Deep Foehn* subtypes (~40 km h^{-1} and ~60 km h^{-1}, respectively), relative humidity varies between below 20% for *Dry Foehn* and above 80% for *Dimmer Foehn*. Regarding the Foehn-induced temperature increase, *Dry Foehn* and *Moist Foehn* exhibit peak values (median of 7.5–8 K), whereas the warming is slightly less pronounced for *Dimmer Foehn* (6.5 K). *Shallow Foehn* emerges as the weakest Foehn flow (mean wind of ~25 km h^{-1}, gusts of ~40 km h^{-1}), as the cross-Alpine pressure difference is also lower compared to the other types. The Foehn-induced warming is additionally reduced (4 K) for *Shallow Foehn* compared to the *Deep Foehn* subtypes. Mean winds (~32 km h^{-1}) and gusts (~55 km h^{-1}) of *Gegenstrom Foehn*, in turn, are only slightly weaker than during *Deep Foehn*. As during *Dimmer Foehn*, elevated relative humidity values are observed (median above 40%), while the warming is likewise less pronounced (4 K).

In this study we focused on Foehn occurring in Altdorf. To what extent our findings apply to other Foehn locations in the Alps remains for future research. As the Foehn types are based upon different synoptic weather situations, they are likely to co-occur at multiple locations. In this regard, a preliminary analysis can be found in the Supplement (Fig. S8). There, the Foehn frequency at various stations across Switzerland (see Table S1) conditioned on Foehn of a certain type in Altdorf is quantified. To this end, Foehn index data as described in Section 2.1 is used at the other stations. The analysis can be interpreted as a first guess whether a location is more or less prone to the occurrence of a certain Foehn type. Foehn frequencies generally

decrease as one moves further down-valley. They also decrease with increasing horizontal distance to the Alpine crest, as well as with increasing altitude difference to major upstream gaps and the respective crest. Besides, specific topographic peculiarities considerably determine the likelihood with which a certain Foehn type occurs at particular stations. In contrast to the evaluation of Foehn types at multiple stations, upstream properties of air parcels are expected to differ substantially depending on the Foehn location. Both Würsch and Sprenger (2015) and Jansing and Sprenger (2022) showed that there exists pronounced valley-to-valley variability, with a much stronger influence of the Po Valley jet for Foehn winds in the Western Alps. Hence, the outcome of the Lagrangian analysis is likely to change if conducted, for example, for the more eastern Rhine Valley.

Furthermore, some caveats are discussed with respect to the data set used in this study. Despite the high resolution, the operational analysis can, similarly to forecasts (Wilhelm et al., 2012; Sandner, 2020), exhibit distinct model biases. For a detailed analysis of these biases, the reader is referred to Tian et al. (2022). Nevertheless, we do not expect near-surface model deficiencies to greatly impact our results, as we mainly focus on mesoscale aspects and refrain from an explicit consideration of local properties in Foehn valleys (e.g., at Altdorf). For the latter, we employ observations instead. With respect to the local-scale impact, a preliminary analysis has been conducted revealing considerable differences in the conditions at Altdorf depending on the prevailing Foehn type (Section 6), as well as an impact on the Foehn occurrence frequency at other stations in Switzerland (Fig. S8). The findings largely correspond to expectations from a forecaster's perspective. In order to explicitly quantify the occurrence of Foehn types at all the stations considered, one would either need additional analysis data, or use the new observational-based Foehn index instead (see Section 2.1).

Additionally, a side note with respect to the Foehn types, as classified in this study, is made. Since the motivation for the different Foehn types arises from the comprehensive existing literature, it is based upon a subjective decision tree. However, the contrasting synoptic conditions of the different Foehn types give confidence in the validity of the methodological approach. The results could be compared to a statistical method, as for example self-organizing maps, an approach chosen by Kusaka et al. (2021) to classify South Foehn in Japan. Naturally, the defined Foehn types are not all-encompassing. Further differentiation between pre-frontal Foehn events and trough Foehn events according to Burri et al. (1999) could be considered. Besides, there exists a rich palette of local Foehn flavors not in the focus of the study. For example, Streiff-Becker (1947) differentiates between different Foehn types for the Canton of Glarus ('Kleintal- and Grosstalfoehn'). Additional, local Foehn winds include the 'Guggifoehn' in the Bernese Alps (Gerstgrasser, 2017), Westfoehn in Lucerne or Eastern Switzerland (Krieger et al., 2018), or the Pfaenderwind at the exit of the Rhine Valley (Gohm et al., 2015).

In summary, the first climatological assessment of Alpine South Foehn types reveals the existence of strikingly different Foehn types, differing with respect to their synoptic to mesoscale characteristics, as well as the upstream air parcel properties. The Foehn types also produce a distinct fingerprint in the local lee-side conditions, a finding valuable for forecasters. Still, open questions with respect to the processes inducing the warming or the mechanisms associated with the descent of the Foehn air remain to be investigated. In a future study, these questions will be tackled using a palette of high-resolution simulations representing all of the different Foehn types.

Code and data availability. Operational MeteoSwiss analyses, as well as measurement data, are available for research purposes upon request to MeteoSwiss. Processed data are available from the authors upon request. The trajectories have been compiled using LAGRANTO (Wernli and Davies, 1997; Sprenger and Wernli, 2015). The code used for the analysis and visualization is written in Python 3.9 and available from the authors upon request.

860

Author contributions. LJ, MS and LP equally contributed to the design of the study and the interpretation of the results. LJ extracted the analysis data from the MeteoSwiss archive, prepared it for the study, and conducted the analysis including the figures in the context of his PhD project. LJ wrote the paper, supported by MS and LP. BD drafted the methods section related to the Foehn index. DG provided input from a forecaster's perspective. All co-authors provided feedback on the paper.

865 *Competing interests.* The authors declare that no competing interests are present.

Acknowledgements. The Swiss National Science Foundation is acknowledged for the funding (SNSF Grant 181992). We want to thank the Federal Office of Meteorology and Climatology MeteoSwiss for providing access to their data archive and the resources used for the data extraction. In particular, Marco Arpagaus and Daniel Leuenberger from MeteoSwiss are acknowledged for additional information related to the COSMO analysis data. In addition, we want to express our thanks to Heini Wernli and Marco Stoll for interesting discussions on several

870   aspects of the study. Besides, we are grateful to our project partners Juerg Schmidli and Yue Tian from Goethe University Frankfurt (GUF) for providing helpful comments during our project meetings, which helped to improve the outcome of the study. Finally, we acknowledge two anonymous reviewers for their thorough reading and their helpful comments, which improved the original manuscript.

References

Baldauf, M., Seifert, A., Förstner, J., Majewski, D., Raschendorfer, M., and Reinhardt, T.: Operational convective-scale numerical weather prediction with the COSMO model: Description and sensitivities, Mon. Weather Rev., 139, 3887–3905, https://doi.org/10.1175/MWR-D-10-05013.1, 2011.

Bougeault, P., Binder, P., Buzzi, A., Dirks, R., Houze, R., Kuettner, J., Smith, R. B., Steinacker, R., and Volkert, H.: The MAP special observing period, B. Am. Meteorol. Soc., 82, 433–462, http://www.jstor.org/stable/26215530, 2001.

Burri, K., Hächler, P., Schüepp, M., and Werner, R.: Der Föhnfall von April 1993, Arbeitsber. MeteoSchweiz, 196, 89 pp., 1999.

Drobinski, P., Steinacker, R., Richner, H., Baumann-Stanzer, K., Beffrey, G., Benech, B., Berger, H., Chimani, B., Dabas, A., Dorninger, M., et al.: Föhn in the Rhine Valley during MAP: A review of its multiscale dynamics in complex valley geometry, Q. J. Roy. Meteorol. Soc., 133, 897–916, https://doi.org/10.1002/qj.70, 2007.

Dürr, B.: Automatisiertes Verfahren zur Bestimmung von Föhn in Alpentälern, Arbeitsber. MeteoSchweiz, 223, 22 pp., 2008.

Elvidge, A. D. and Renfrew, I. A.: The causes of foehn warming in the lee of mountains, B. Am. Meteorol. Soc., 97, 455–466, https://doi.org/10.1175/BAMS-D-14-00194.1, 2016.

Elvidge, A. D., Renfrew, I. A., King, J. C., Orr, A., Lachlan-Cope, T. A., Weeks, M., and Gray, S. L.: Foehn jets over the Larsen C ice shelf, Antarctica, Q. J. Roy. Meteorol. Soc., 141, 698–713, https://doi.org/10.1002/qj.2382, 2015.

Ficker, H.: Über die Entstehung der Föhnwinde auf der Nordseite der Alpen (On the formation of foehn winds on the northern side of the Alps), Meteorol. Z., p. 439–451, https://doi.org/10.1127/0941-2948/2012/0532, translated and edited by Volken E. and S. Brönnimann. – Meteorol. Z. 21 (2012), 597–605, 1910.

Ficker, H.: Warum steigt der Föhn in die Täler herab, Meteorol. Z, 48, 227–229, 1931.

Frey, K.: Der «Jahrhundertföhn» vom 8. November 1982, Meteorol. Rundschau, 37, 209–220, 1984.

Frey, K.: Entwicklung und Eigenschaften des Südföhns: Beitrag für ein modifiziertes Föhnmodell, Geographica Helvetica, 47, 57–63, 1992.

Frey, K.: Geheimnisvoller Föhn: Beschreibungen-Wissenschaftliches-Merkwürdiges, Mitt. Naturforsch. Ges. Kt. Solothurn, 40, 65–88, 2007.

Gerstgrasser, D.: Dokumentation Südföhn, MeteoSwiss internal report. 59 pp. [available from the authors upon request], 2017.

Gohm, A. and Mayr, G.: Hydraulic aspects of föhn winds in an Alpine valley, Q. J. Roy. Meteorol. Soc., 130, 449–480, https://doi.org/10.1256/qj.03.28, 2004.

Gohm, A., Siller, M., and Bär, J.: Nature and climatology of Pfänderwind, Meteorol. Z., 24, 243–259, https://doi.org/10.1127/metz/2015/0648, 2015.

Gubser, S.: Wechselwirkung zwischen Föhn und planetarer Grenzschicht, Ph.D. thesis, ETH Zurich, https://doi.org/10.3929/ethz-a-005207902, 2006.

Gutermann, T., Dürr, B., Richner, H., and Bader, S.: Föhnklimatologie Altdorf: Die lange Reihe (1864-2008) und ihre Weiterführung, Vergleich mit anderen Stationen, Arbeitsber. MeteoSchweiz, 241, 53 pp., https://doi.org/10.3929/ethz-a-007583529, 2012.

Güller, A.: Der aussergewöhnliche Föhnsturm vom 13. Februar 1976 in der Ostschweiz, Arbeitsbericht der Schweiz. Met. Zentralanstalt, 69, 16 pp., 1977.

Hächler, P., Burri, K., Dürr, B., Gutermann, T., Neururer, A., Richner, H., and Werner, R.: Der Föhnfall vom 8. Dezember 2006–eine Fallstudie, Arbeitsber. MeteoSchweiz, 234, https://doi.org/10.3929/ethz-a-007319165, 2011.

Hann, J.: Zur Frage über den Urpsrung des Föhn, Z. Oester. Ges. Meteorol., 1, 257–263, 1866.

Hann, J.: Einige Bemerkungen zur Entwickelungs-Geschichte der Ansichten über den Ursprung des Föhn, Meteorol. Z., 20, 393–399, 1885.

910   Hann, J.: Lehrbuch der Meteorologie, VDM Verlag Dr. Müller, 1901.

Jansing, L. and Sprenger, M. i. p.: Thermodynamics and airstreams of a South Foehn event in different Alpine valleys, Q. J. Roy. Meteorol. Soc., pp. 1–32, https://doi.org/10.1002/qj.4285, 2022.

Kanitscheider, R.: Beiträge zur Mechanik des Föhns, Beitr. Phys. fr. Atm., 18, 27–49, 1932.

Krieger, N., Sprenger, M. A., and Müller, E.: Westföhn am Vierwaldstättersee, Fachber. MeteoSchweiz, 269, 2018.

915   Kuhn, W.: Rudolf Streiff-Becker als Föhnforscher, Mitt. Naturforsch. Ges. Kt. Glarus, XIV, 25–47, 1984.

Kusaka, H., Nishi, A., Kakinuma, A., Doan, Q.-V., Onodera, T., and Endo, S.: Japan's south foehn on the Toyama Plain: Dynamical or thermodynamical mechanisms?, Int. J. Climatol., 41, 5350–5367, https://doi.org/10.1002/joc.7133, 2021.

Lehmann, O.: Zur Geschichte der Föhntheorie, Vierteljahresschr. Naturforsch. Ges. Zürich, p. 45–76, 1937.

Mayr, G., Armi, L., Arnold, S., Banta, R. M., Darby, L. S., Durran, D., Flamant, C., Gaberšek, S., Gohm, A., Mayr, R., et al.: Gap flow
920   measurements during the Mesoscale Alpine Programme, Meteorol. Atmos. Phys., 86, 99–119, https://doi.org/10.1007/s00703-003-0022-2, 2004.

Mayr, G. J. and Armi, L.: Föhn as a response to changing upstream and downstream air masses, Q. J. Roy. Meteorol. Soc., 134, 1357–1369, https://doi.org/10.1002/qj.295, 2008.

Mayr, G. J., Armi, L., Gohm, A., Zängl, G., Durran, D. R., Flamant, C., Gaberšek, S., Mobbs, S., Ross, A., and Weissmann, M.: Gap flows:
925   results from the Mesoscale Alpine Programme, Q. J. Roy. Meteorol. Soc., 133, 881–896, https://doi.org/10.1002/qj.66, 2007.

Medina, S. and Houze, R. A.: Air motions and precipitation growth in Alpine storms, Q. J. Roy. Meteorol. Soc., 129, 345–371, https://doi.org/10.1256/qj.02.13, 2003.

Miltenberger, A. K., Pfahl, S., and Wernli, H.: An online trajectory module (version 1.0) for the nonhydrostatic numerical weather prediction model COSMO, Geosci. Model Dev., 6, 1989–2004, https://doi.org/10.5194/gmd-6-1989-2013, 2013.

930   Miltenberger, A. K., Reynolds, S., and Sprenger, M.: Revisiting the latent heating contribution to foehn warming: Lagrangian analysis of two foehn events over the Swiss Alps, Q. J. Roy. Meteorol. Soc., 142, 2194–2204, https://doi.org/10.1002/qj.2816, 2016.

Richner, H. and Dürr, B.: Facts and fallacies related to dimmerfoehn, Tech. rep., ETH Zurich, https://doi.org/10.3929/ethz-a-010439615, 2015.

Richner, H. and Hächler, P.: Understanding and forecasting Alpine Foehn, in: Mountain Weather Research and Forecasting, edited by Chow,
935   F. K., De Wekker, S. F., and Snyder, B. J., chap. 4, pp. 219–260, Springer Atmospheric Sciences, https://doi.org/10.1007/978-94-007-4098-3, 2013.

Richner, H., Baumann-Stanzer, K., Benech, B., Berger, H., Chimani, B., Dorninger, M., Drobinski, P., Furger, M., Gubser, S., Gutermann, T., et al.: Unstationary aspects of foehn in a large valley part I: operational setup, scientific objectives and analysis of the cases during the special observing period of the MAP subprogramme FORM, Meteorol. Atmos. Phys., 92, 255–284, https://doi.org/10.1007/s00703-005-
940   0134-y, 2006.

Richner, H., Dürr, B., Gutermann, T., and Bader, S.: The use of automatic station data for continuing the long time series (1864 to 2008) of foehn in Altdorf, Meteorol. Z., 23, 159–166, https://doi.org/10.1127/0941-2948/2014/0528, 2014.

Rotunno, R. and Houze, R. A.: Lessons on orographic precipitation from the Mesoscale Alpine Programme, Q. J. Roy. Meteorol. Soc., 133, 811–830, https://doi.org/10.1002/qj.67, 2007.

945   Saigger, M.: Is it North or West Foehn? A Lagrangian Analysis of PIANO IOP 1, Master's thesis, University of Innsbruck, https://diglib.uibk.ac.at/urn/urn:nbn:at:at-ubi:1-94032, 2021.

Saigger, M. and Gohm, A.: Is it north or west foehn? A Lagrangian analysis of Penetration and Interruption of Alpine Foehn intensive observation period 1 (PIANO IOP 1), Weather Clim. Dyn., 3, 279–303, https://doi.org/10.5194/wcd-3-279-2022, 2022.

Sandner, V.: Verification of COSMO-1 forecasts of foehn breakthrough and interruption in the region of Innsbruck, Master's thesis, University of Innsbruck, https://resolver.obvsg.at/urn:nbn:at:at-ubi:1-65459, 2020.

Schär, C., Fuhrer, O., Arteaga, A., Ban, N., Charpilloz, C., Di Girolamo, S., Hentgen, L., Hoefler, T., Lapillonne, X., Leutwyler, D., et al.: Kilometer-scale climate models: Prospects and challenges, B. Am. Meteorol. Soc., 101, E567–E587, https://doi.org/10.1175/BAMS-D-18-0167.1, 2020.

Schneidereit, M. and Schär, C.: Idealised numerical experiments of Alpine flow regimes and southside precipitation events, Meteorol. Atmos. Phys., 72, 233–250, https://doi.org/10.1007/s007030050018, 2000.

Schraff, C. H.: Mesoscale data assimilation and prediction of low stratus in the Alpine region, Meteorol. Atmos. Phys., 64, 21–50, https://doi.org/10.1007/BF01044128, 1997.

Seibert, P.: South foehn studies since the ALPEX experiment, Meteorol. Atmos. Phys., 43, 91–103, https://doi.org/10.1007/BF01028112, 1990.

Seibert, P.: Hann's thermodynamic foehn theory and its presentation in meteorological textbooks in the course of time, From Beaufort to Bjerknes and Beyond, Algorismus, 52, 169–180, 2005.

Smith, R. B.: The influence of mountains on the atmosphere, in: Adv. Geophys., vol. 21, pp. 87–230, Elsevier, https://doi.org/10.1016/S0065-2687(08)60262-9, 1979.

Sprenger, M. and Schär, C.: Rotational aspects of stratified gap flows and shallow föhn, Q. J. Roy. Meteorol. Soc., 127, 161–187, https://doi.org/10.1002/qj.49712757110, 2001.

Sprenger, M. and Wernli, H.: The LAGRANTO Lagrangian analysis tool–version 2.0, Geosci. Model Dev., 8, 2569–2586, https://doi.org/10.5194/gmd-8-2569-2015, 2015.

Sprenger, M., Dürr, B., and Richner, H.: Foehn studies in Switzerland, in: From weather observations to atmospheric and climate sciences in Switzerland, edited by Willemse, S. and Furger, M., chap. 11, pp. 215–248, vdf Hochschulverlag AG, Zurich, 2016.

Steinacker, R.: Alpiner Föhn – eine neue Strophe zu einem alten Lied, Promet, 32, 3–10, 2006.

Stephan, K., Klink, S., and Schraff, C.: Assimilation of radar-derived rain rates into the convective-scale model COSMO-DE at DWD, Q. J. Roy. Meteorol. Soc., 134, 1315–1326, https://doi.org/10.1002/qj.269, 2008.

Steppeler, J., Doms, G., Schättler, U., Bitzer, H., Gassmann, A., Damrath, U., and Gregoric, G.: Meso-gamma scale forecasts using the nonhydrostatic model LM, Meteorol. Atmos. Phys., 82, 75–96, https://doi.org/10.1007/s00703-001-0592-9, 2003.

Streiff-Becker, R.: Die Föhnwinde, Vierteljahresschr. Naturforsch. Ges. Zürich, 78, 66–82, 1933.

Streiff-Becker, R.: Der Dimmerföhn, Vierteljahresschr. Naturforsch. Ges. Zürich, 92, 195–198, 1947.

Tian, Y., Duarte, J. Q., and Schmidli, J.: A station-based evaluation of south foehn forecasting with COSMO-1, to be submitted, 2022.

Walker, A. and Ruffner, H.: Föhnforschung und Traubenreife, Schweiz. Z. Obst-Weinbau, pp. 245–247, 1998.

Wastl, C., Schunk, C., Lüpke, M., Cocca, G., Conedera, M., Valese, E., and Menzel, A.: Large-scale weather types, forest fire danger, and wildfire occurrence in the Alps, Agr. Forest Meteorol., 168, 15–25, https://doi.org/10.1016/j.agrformet.2012.08.011, 2013.

Wernli, H. and Davies, H. C.: A Lagrangian-based analysis of extratropical cyclones. I: The method and some applications, Q. J. Roy. Meteorol. Soc., 123, 467–489, https://doi.org/10.1002/qj.49712353811, 1997.

Wilhelm, M., Buzzi, M., Sprenger, M., and Hächler, P.: COSMO-2 model performance in forecasting foehn: A systematic process-oriented verification, Master's thesis, Bundesamt für Meteorologie und Klimatologie, MeteoSchweiz, 2012.

985   Würsch, M. and Sprenger, M.: Swiss and Austrian foehn revisited: A Lagrangian-based analysis, Meteorol. Z., 24, 225–242, https://doi.org/10.3929/ethz-b-000103254, 2015.

Zängl, G.: North foehn in the Austrian Inn Valley: A case study and idealized numerical simulations, Meteorol. Atmos. Phys., 91, 85–105, https://doi.org/10.1007/s00703-004-0106-7, 2006.

Zängl, G. and Hornsteiner, M.: The exceptional Alpine south föhn event of 14–16 November 2002: A case study, Meteorol. Atmos. Phys.,
990   98, 217–238, https://doi.org/10.1007/s00703-006-0257-9, 2007.

Zumbrunnen, T., Bugmann, H., Conedera, M., and Bürgi, M.: Linking forest fire regimes and climate—a historical analysis in a dry inner Alpine valley, Ecosystems, 12, 73–86, https://doi.org/10.1007/s10021-008-9207-3, 2009.